Damage Detection in Composites using E-glass Fibre and Small Diameter Optical Fibre

by

Samuel Olukunle Ojo

A dissertation submitted to the
University of Birmingham
for the degree of

Master of Research

School of Metallurgy and Materials
College of Engineering and Physical Sciences
University of Birmingham
January 2011

Abstract

The primary aim of this study was to demonstrate that E-glass and custom-made small diameter optical fibres, with an outer diameter of 12 micrometres, can be used to monitor the following: (i) *In-situ* monitoring of the partial dissolution of the cladding on the small-diameter optical fibres in hydrofluoric acid. This was necessary for the small-diameter optical fibres as the thickness of the original cladding was not appropriate to enable evanescent wave spectroscopy. (ii) *In-situ* monitoring of the impregnation process. Since the cladding was etched to access the evanescent field in the optical fibres, it was demonstrated that the impregnation of the fibres by the resin could be monitored. (iii) *In-situ* cure monitoring. After impregnation, the cross-linking reactions taking place at the surface of the glass fibres were monitored using near-infrared spectroscopy. The feasibility of using the glass fibres for monitoring temperature was also demonstrated. (iv) Finally, after the composite was cured, it was tensile tested to failure whilst monitoring the transmitted light intensity through the optical fibres. The un-impregnated bundles were also tensile tested to failure. The failure of the individual filament in the bundle (un-impregnated) and composites were monitored by tracking the intensity of the transmitted light through each filament. Conventional acoustic emission was used to cross-correlate the fracture of the individual filaments. Conventional E-glass fibres can be used as light guides if the conditions for total internal reflection is enabled. In this current study, the matrix served as the cladding.

This study has developed a range of techniques that can potentially facilitate the full life cycle monitoring of glass fibre composites. In other words, the same test specimen can be used to monitoring the surface treatment, temperature during drying or heat treatment,

cross-linking kinetics and damage during mechanical loading. The self-sensing technique developed in this study can also be used as a tool to study the degradation of properties when the fibres are recycled and reused.

Dedication

This thesis is dedicated to my heavenly Father, God Almighty, my Saviour, Jesus Christ and my greatest teacher, the Holy Spirit. He is the Alpha and the Omega, the beginning and the end.

Acknowledgements

During the time of working on this piece of research work at the University of Birmingham, several persons contributed directly and indirectly to my success especially the Sensors and Composites group of the School of Metallurgy and Materials. Without their support it would be impossible for me to finish my work. That is why I wish to dedicate this section to recognise their support.

I want to start by expressing a sincere acknowledgement to my advisors Dr. Liwei Wang and colleague Mr. Shoaib Malik who gave me the opportunity to research under their guidance and supervision. I received motivation, encouragement, inspiration and support from them during my studies here. I also wish to thank Dr. Ramani Salmalee Mahendran for the example, inspiration, guidance and support I received from her. Special thanks I owe Prof. Gerard Franklin Fernando for the opportunity he has offered me to research under his supervision, his unrivalled support, guidance, constructive criticism and transmitted knowledge for the completion of this work. His motivation and encouragement from the preliminary to the concluding level enabled me to develop an understanding of the subject.

I also like to express my gratitude to the EPSRC for providing the grant funding and resources used for the development of this research. At last, my sincere gratitude to my family, friends and Church brethren especially my wife, Deacs. Stella Omotayo Ojo and my Pastor, Grace Edem for their prayers, unconditional support and love. Mo ki yin, ẹ se e pupọ.

Table of Contents

Figure	List of Figures	Page

Table	List of Tables	Page

Chapter 1

1.0 Introduction

In recent years, there has been a rising global demand for, and interest in, developing techniques that are capable of monitoring the structural integrity of composites. Structural monitoring techniques is important for engineers as it will have the ability to reveal inherent gross flaws or damage that can cause catastrophic failure of the composite [2] .

Various test methods have been developed for assessing the mechanical, physical, and thermal properties of fibre reinforced composites [3], [4]. A range of non-destructive evaluation (NDE) techniques are also used to assess the properties of composites. Non-destructive testing (NDT) can provide a viable means of detecting damage due to impact damage, cyclic fatigue and environmental exposure of critical structures. In addition, there are unexpected damage events that can occur during the life of a composite. Example of this are: accidental impacts, de-laminations, drastic environmental changes, and loading conditions. Therefore, it is important for engineers to be able to monitor the structural integrity of these critical structures during their lifetimes rather than conducting routine inspections whilst out of service. NDT and remote monitoring can reduce maintenance costs, improve safety/reliability, and predict the remaining life expectancy of the structures [5], [6]

Progress has also been reported in recent years on developing *in-situ* non-destructive test (NDT) techniques, for example, self-sensing composites [7]. Although the use of optical fibre sensors have made a significant impact in the real-time process monitoring of

engineering materials and structures, there are concerns with regard to the diameter mismatch between the reinforcing fibres and the embedded sensor [8]. This mismatch in the diameter (Figure 1.1) can have a detrimental effect on relative orientation of the reinforcing fibres [9].

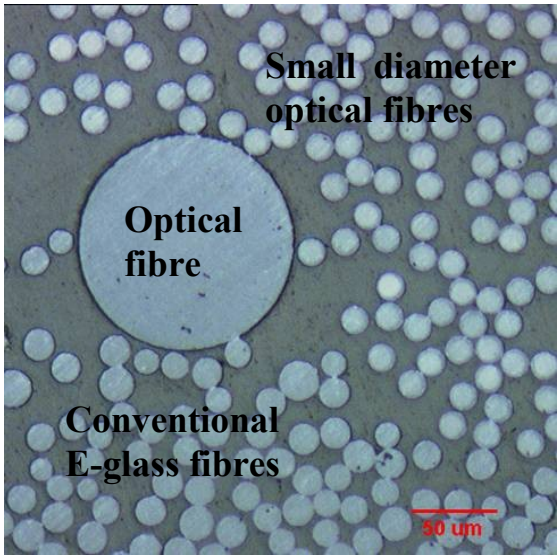

Figure 1.1: Optical micrograph of a fibre bundle showing conventional E-glass fibre, small diameter optical fibre (SDOF) and 125 μm diameter multimode optical fibre.

1.1 Aims

The primary aims of this project are:

(i) to develop a manufacturing technique to enable the production of void-free self-sensing composites.

A resin injection system and a closed-mould was designed and developed to enable the production of void free composite. The quality of the composite was assessed using conventional image analysis-based technique;

(ii) to investigate whether the impregnation process can be monitored via the transmitted light intensity through reinforcing glass fibres.

At present, it is not possible to monitor the impregnation of reinforcing fibre bundle *in-situ*. This study developed a technique that can be used to monitor the transmitted light intensity during the impregnation process;

(iii) to monitor the cross-linking process using impregnated fibre bundles.

The same fibre bundle used for monitoring impregnation was used to monitor the cross-linking process using evanescent wave spectroscopy; and

(iv) to study the failure of the reinforcing fibres in real-time during tensile testing using high-speed photography.

Having monitored the impregnation process and the cross-linking of the fibre bundle, the same specimen was subjected to tensile loading in order to determine the fracture of individual filament in real-time using a high-speed camera.

The term 'self-sensing' is used here to describe the situation where the reinforcing fibres are themselves used as light guides. Embedded optical fibres can also be considered as a foreign material with a potential to cause undesired effects. For example, delaminations, waviness, debondings, porosity, and variation in the fibre volume content (resin-rich or resin-depleted areas) [10].

The possibility of converting reinforcing E-glass fibres as waveguides, offers the potential to exploit the material as sensors. In addition to using E-glass fibre waveguides for monitoring the damage incurred in composite during mechanical testing, waveguides can also be used to monitor the changes in the refractive index of the cladding or matrix during the cross-linking process. E-glass fibre waveguides also offer the potential for detecting impact-induced damage in composites. This approach of using the reinforcing E-glass

fibres is cost-effective, as the technology only requires a light source and detector. It is also reliable since the reinforcing fibre serves as the sensor [11].

Chapter 2

Literature Review

2.0 Introduction

The use of fibre reinforced composite materials present a radical approach to designing structural materials when compared with the more traditional use of metals and ceramics [12]. A wide range of reinforcements, mainly in fibrous form, are commercially available. Their properties can be related to the molecular structure and the defect contents of the reinforcements, both of which must be controlled during the manufacturing stage [13].

Fibre reinforced composite materials are being used as a structural material in many manufacturing sectors. Reinforced composites offer high strength-to-weight ratio and durability and they are used widely in a number of industrial sectors. Synthetic fibres continue to gain prominence and preference in various industries in comparison with other traditional materials because of their characteristic properties [14], [15]; these include:

(i) High tensile strength.

(ii) High tensile modulus.

(iii) High toughness (depending on the type).

(iv) Resistance to abrasion.

(v) Relative insensitivity to moisture.

(vi) Low density.

(vii) Good vibration resistance.

(viii) Low linear coefficient of thermal expansion.

(ix) Good wear, fatigue and electro-magnetic resistance.

(x) High insulation capability.

(xi) Good electrical insulation (depending on the type of reinforcement).

2.1 Types of Fibre Reinforcements

Many types of reinforcements are now commercially available but in general, they are designed for a particular matrix system. A selection of the reinforcements is listed in Table 2.1, and their properties are as listed in Table 2.2. All of these fibres have a high stiffness and relatively low density, which makes them ideal for manufacturing lightweight composite structures. Carbon, glass and aramid fibres are used extensively in polymer composites whilst ceramic fibres, whiskers, and particles are being used to reinforce metal and ceramic matrices [13].

The basic mechanical properties of selected fibres are given in Table 2.2. The surface interaction between the fibres and resin matrix is controlled by the degree of bonding that exists between the two. This in turn is heavily influenced by the treatment given to the fibre surface, a description of the different surface treatments and 'finishes' is also discussed in section 2.2.1.1.

Table 2.1: Some common types of reinforcements [13].

Form	Size (μm)		Fabrication route	Example
	D	L		
Monofilaments (large-diameter single fibres)	100-150	∞	CVD onto core fibres (e.g. of c or W)	SiC (SCS-6™) Boron
Multifilaments (tows or woven rovings with up to 14000 fibres per strand)	7-30	∞	Precursor stretching; pyrolysing; melt spinning	Carbon (HS & HM) Glass Nicalon™ Kevlar™ 49 FP™ alumina
Short fibres (staple fibres aggregated into blankets, tapes, wool, etc)	1-10	50-5000	Spinning of slurries or solutions, heat treatment	Saffil™ Kaowool Fibrefrax™
Whiskers (fine single crystals in loose aggregates)	0.1-1	5-100	Vapour phase growth/reaction	SiC Al_2O_3
Particulates (loose powder)	5-20	5-20	Steelmaking byproduct; refined ore; sol-gel processing, etc.	SiC Al_2O_3 B_4C TiB_2

D – fibre diameter.
L – fibre length.

Table 2.2: Fibre properties [13].

Fibre	Density	Young's modulus	Poisson's ratio	Tensile strength	Failure strain	Thermal expansivity	Thermal conductivity
	Kgm^{-3}	GPa		GPa	%	$10^{-6}K^{-1}$	$Wm^{-1}K^{-1}$
SiC Mono-filament	$3x10^{-6}$	400	0.20	2.4	0.6	4.0	10
Boron Mono-filament	$2.6\ x10^{-6}$	400	0.20	4.0	1.0	5.0	38
HM[a] carbon	$1.95\ x10^{-6}$	Axial 380 Radial 12	0.20	2.4	0.6	Axial– 0.7 Radial 10	Axial 105
HS[b] carbon	$1.75\ x10^{-6}$	Axial 230 Radial 20	0.20	3.4	1.1	Axial-0.4 Radial 10	Axial 24
E-glass	$2.56\ x10^{-6}$	76	0.22	2.0	2.6	4.9	13
Nicalon™	$2.6\ x10^{-6}$	190	0.20	2.0	1.0	6.5	10
Kevlar™ -49	$1.45\ x10^{-6}$	Axial 130 Radial 10	0.35	3.0	2.3	Axial -6 Radial 54	Axial 0.04
FP™ fibre	$3.9\ x10^{-6}$	380	0.26	2.0	0.5	8.5	8
Saffil™	$3.4\ x10^{-6}$	300	0.26	2.0	0.7	7.0	5
SiC whisker	$3.2\ x10^{-6}$	450	0.17	5.5	1.2	4.0	100
Cellulose (flax)	$1.0\ x10^{-6}$	80	0.3	2.0	3.0	-	-

[a]High modulus.
[b]High strength.

The focus of this MRes thesis is on E-glass fibres and therefore the other classes of reinforcement cited in Table 2.2 are not discussed.

2.2 Glass Fibres

There are considerable numbers of glass fibre types available. The composition of the commonly used glass fibre is given in Table 2.3 [16]. Glass filaments are relatively low-cost when compared to other reinforcing fibres (see Figure 2.1) and readily available reinforcement with high ultimate tensile strengths (see Table 2.4) [17], [18], [19], [20].

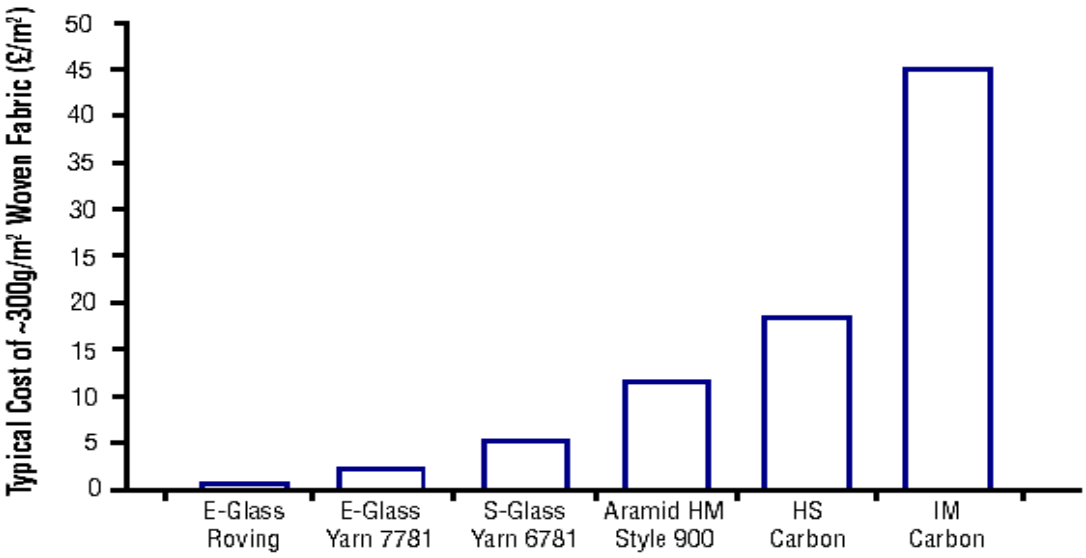

Figure 2.1: Comparative fibre cost
(Source:http://www.bolton.ac.uk/CODATE/SPGuidetoComposites.pdf).

Fine, high strength, glass fibres are produced by blending quarry products comprising mainly sand, limestone and colemanite at about 1600 ^{o}C to form molten glass. This molten glass is subsequently passed through micro-fine bushings and simultaneously cooled down to produce glass fibre filaments with diameters ranging from 5 - 24 μm [20], [18].

Figure 2.2: Photographs of a creel E-glass fibre supplied by PPG, U.K.

A typical composition of the commonly used glass fibre is given in Table 2.3.

Table 2.3: Typical composition for E, A, C, M, and S-glass fibres [18].

	Weight Percent						
	SiO_2	**Al_2O_3**	**CaO**	**MgO**	**B_2O_3**	**Na_2O**	**Others**
E-glass	54	14	19	2	10	1	K_2O, TiO_2, Fe_2O_3, F_2
A-glass	72	1	10	2		14	SO_3 1 %
C-glass	65	4	14	3	5.5	8	K_2O 0.5 %
M-glass	54		13	9			BeO 8 %, TiO_2 8 %, CeO_2, Li_2O, ZrO_2, Fe_2O_3
S-glass	65	25		10			

Table 2.4 presents a summary of the properties of various grades of glass fibres available commercially.

Table 2.4: Glass fibres: summary of properties of relevance to fibre reinforcement [18].

	Relative Cost (*)	Young's Modulus (GN/m^2)	Ultimate Tensile Strength (GN/m^2)	Specific Gravity	Strain Point (K)	Remarks
E-glass	0.2	72	3.400	2.54	889	Most readily available fibre
A-glass	0.2	70	3.200	2.50	800	Common soda-lime glass
C-glass	1	69	3.100	2.49	825	Corrosion-resistant
D-glass	3	52	2.400	2.16	748	High dielectric constant glass
M-glass	2	110	3.400	2.89	800	High modulus
S-glass	0.5	85	4.800	2.48	1033	Developed to give higher strength than E-glass
Fused SiO_2	5	73	7.000	2.20	1343	

* Steel wire = 1 per unit of weight.

Strain point is a measure of temperature capability, being the temperature at which the viscosity is $10^{13.5}Ns/m^2$.

Costs and properties are dependent on fibre diameter; comparable representative figures are given.

2.2.1 E-glass fibres

E-glass means electrically graded glass and was originally developed for use in stand-off insulators in high-tension electrical wiring. It was later found to have excellent fibre forming capabilities, and they are used extensively as the reinforcing material in glass fibre composites

An ultimate strength of approximately 3.5 GPa has been measured for E-glass fibres but flaws from contact abrasion and hydrolytic degradation are typically present in mass produced fibres [21]. Also, the interaction of moisture with metal oxides, can lead to corrosion-induced defects; this can influence the interfacial bond strength between the fibre and the matrix and reduce the durability and mechanical strength of E-glass fibre-matrix bonds [22]. Some of the oxides in glass, such as, SiO_2, Fe_2O_3, and Al_2O_3, form links to hydroxyl groups during contact with water which in turn form hydrogen bonds with water molecules. With time, this may cause leaching of elements such as Na and Ca, which leave a weak and porous surface. The presence of water also reduces the wettability of the fibres, which reduces the interfacial shear strength [23].

2.2.1.1 Surface treatment

A procedure called "sizing" is usually carried out during fibre manufacturing; this is a surface treatment primarily employed to improve the wettability of the fibre surfaces with respect to the liquid resins used as the matrix. This is said to improve the durability and mechanical strength of the fibre-matrix bond and these are usually termed as coupling agent [13]. The sizing agent is generally a water-based mixture containing a lubricant, a film former, and a coupling agent applied from an aqueous emulsion [21], [24].

A typical example is silane coatings, which functions as coupling agent and are applied to provide a strong chemical link between the hydroxyl groups on the fibre surface and the polymer molecules of the resin. Silane coupling agents have the general chemical formula R-Si-X_3. This is a multifunctional molecule, which reacts with the glass surface at one end and polymer phase at the other end. The X units represent hydrolysable groups such as the

ethoxy group (-OC_2H_5). The silane is hydrolysed to the corresponding silanol as schematically displayed in Figure 2.3 [13].

Thomas [25], [26], [27], [28] carried out a series of experiments to investigate the effect of surface treatment, fibre diameter, gauge length, and strain rate on the strength of glass fibre bundles. He concluded that an increase in surface area make the fibre susceptible to surface damage whilst longer gauge length have the tendency of increasing the probability for critical flaws. Thomas also noted that there was an increase of about 59 % in bundle tensile strength when glass fibre was coated with wax and a 90 % increase when coated with polyester. He attributed this increase in strength to a reduction in contact abrasion and increase in the load transfer efficiency due to the coating.

In another study, it was discovered that coating a single strand of fibre with silane treatment agent increases its strength by approximately 18 % [29]. Also it was found that coating glass fibre bundle with lubricating oil increases its tensile strength by 14 % [30]. Katzmann (1987) as reported by Hull and Clyne, found out that in some systems where wetting is very poor, coatings were used for improving interfacial bonding.

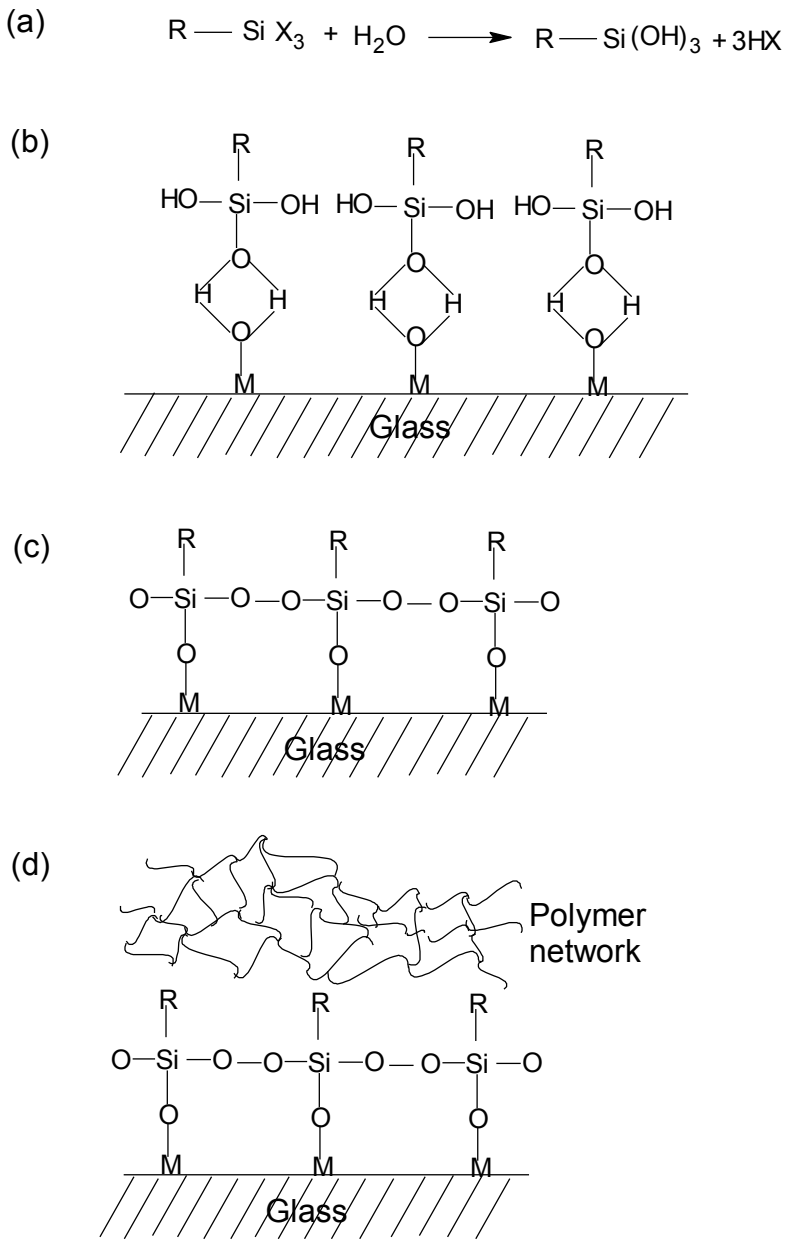

Figure 2.3: Silane coupling agents (a) hydrolysis of an organo-silane to the corresponding silanol, (b) hydrogen bonding between hydroxyl groups of the silanol and those attached to the glass surface, (c) polysiloxane bonded to the glass after condensation reactions during and (d) bonding between the functional group R and the polymer matrix [13].

2.3 Matrices

These are materials commonly used in composites manufacture; they are usually plastic materials that are relatively cheaper to produce when compared with the reinforcing fibres themselves. Epoxy resin is commonly used matrix in basic composite manufacturing, but other materials that have desirable properties are also available [31].

2.3.1 Properties of matrices

Any resin to be used in composite manufacturing will need to have good mechanical, adhesives, and toughness properties. Good resistance to environmental degradation is also desirable. Table 2.5 shows selected list of matrices used for manufacturing composite with their properties.

Table 2.5: Common matrix properties [32].

Matrix		**Density (g/mm^3)**	**Tensile Strength at 23 ^{0}C (N/mm^2)**	**E-Modulus at 23 ^{0}C (N/mm^2)**
UP	Cold cured	1200	70	3,500
	Warm cured	1200	60	3,500
EP	Cold cured	1200	70	3,500
	Warm cured	1200	90	3,500
PEEK		1300	100	3,800

UP: Unsaturated Polyester Resin (Thermoset)
EP: Epoxy Resin (Thermoset)
PEEK: Polyetheretherketone (Thermoplastic)

The matrix is responsible for binding together the surfaces of reinforcing fibre filament. The constituent of this material is predominantly based on synthetic polymers, which is generally a low-viscosity liquid used to impregnate fibre surfaces to allow for maximum bonding interactions. The actual bonding forms as the adhesive undergoes cross-linking (i.e. a liquid-to-solid transition) which may be accomplished through either a physical

process (e.g. crystallization, solvent evaporation) or a chemical process (e.g. addition polymerization, condensation, etc). Characteristics of a "good" bond should include high shear, peel and fracture strengths. High adhesion is required between reinforced fibres and the matrix. This will ensure efficient load-transfer and prevent fibres-resins de-bonding when stressed [33].

Furthermore, the matrix must have good resistance to the environment, water, and other aggressive substances and an ability to withstand constant stress-cycling particularly when used in a marine or swamp area (e.g. bridge construction).

2.3.2 Types of matrices

Polymers can be classified as one of two types, 'thermoplastic' and 'thermosetting', according to the effect of heat on their properties. Thermoplastics soften with heating and eventually melt, hardening again on cooling, whereas the thermosetting process is irreversible [34].

2.3.2.1 Epoxy resin

This is a monomer that hardens when crosslinked with a variety of hardeners (cross-linking agent) due to the existence of high reactivity of the strained epoxide ring (the structure is as shown in Figure 2.6) in the system. It is commonly seen as a "two-part" epoxy-resin adhesive (the general reactions are as illustrated in Figure 2.8). Typical examples of epoxy resins are DGEBA, TGDDM and TGAP (the structures are as shown in Figures 2.5, 2.6, and 2.7 respectively). They are widely used in many applications, such as, coatings, as structural adhesives, microelectronics, and as a matrix in composites manufacturing. Epoxy resins are often used as the matrix phase in fibreglass and carbon fibre reinforced plastic

(CFRP) composites. Using epoxy resin is more expensive than polyester resins and vinyl ester resins, but it generally produces stronger, high temperature resistant materials [35], [36], [24], [34].

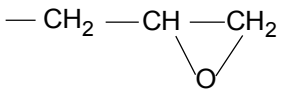

Figure 2.4: Structure of an Oxirane ring [36].

2.3.2.2 Curing agents

Due to the high operating temperature encountered and high mechanical strengths needed in some applications like aerospace, epoxy resins based on tetraglycidyl-4,4' diaminodiphenylmethane (TGDDM or TGMDA) have been found to be suitable. These are usually cured with diaminodiphenylsulphone (DDS) and/or boron trifluoride monoethylamine (BF3-MEA) for use as a matrix material in advanced composites. Epoxy resins are usually used as matrix resins since they can be used to produce prepregs that can be cured at relatively low temperatures (120 ^{0}C and 180 ^{0}C). The extent of shrinkage due to curing is relatively low. Other curing agents available are: dicyandiamide and derivatives, aliphatic amines, polyimide resins and derivatives, acid anhydrides, etc [37].

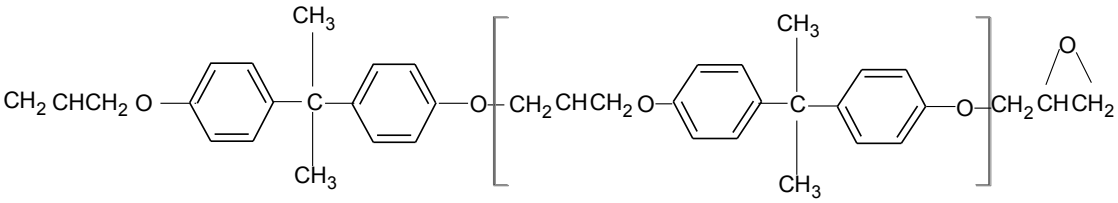

With n = 0.12

Di-Glycidyl Ether of Bisphenol A (DGEBA)

DDS: 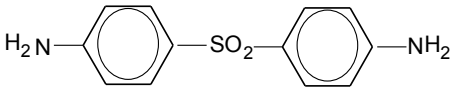

Figure 2.5: Structure of Di-Glycidyl Ether of Bisphenol A (DGEBA) and DDS [36].

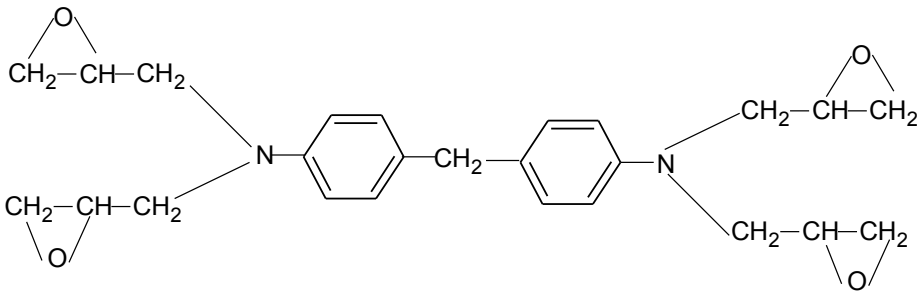

Tryglycidyl p-amino phenol and diglycidyl -4-4-diamino-diphenylmethane (TDDM)

Figure 2.6: Structure of Tryglycidyl p-amino phenol and diglycidyl -4-4-diamino diphenylmethane (TDDM) [36].

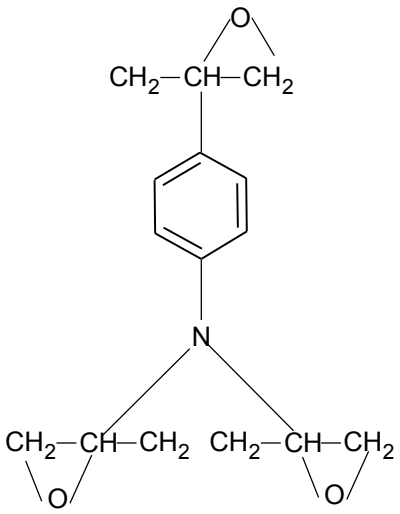

Triglycidyl p-amino phenol (TGAP)

Figure 2.7: Structure of Triglycidyl p-amino phenol (TGAP) [36].

2.3.2.3 Epoxy-amine cross-linking

Crosby and Fernando [34] reported that there are generally two accepted reactions which occur during epoxy-amine cure reactions. The reaction commences when the initially existed primary amine in the system react with epoxide ring to produce secondary amine and hydroxyl groups (the structure is as shown in Figure 2.8 (i)). Further reaction of the secondary amine groups with the epoxide ring forms the tertiary amine groups (the reaction is as shown in Figure 2.8 (ii)). They also reported that addition reactions of epoxy to primary or secondary amine groups are catalysed by acids such as Lewis acids, phenols, and alcohols. Hydroxyl groups formed by these reactions also acts as catalyst, which means that autocatalysis does occur during the early stage of cure.

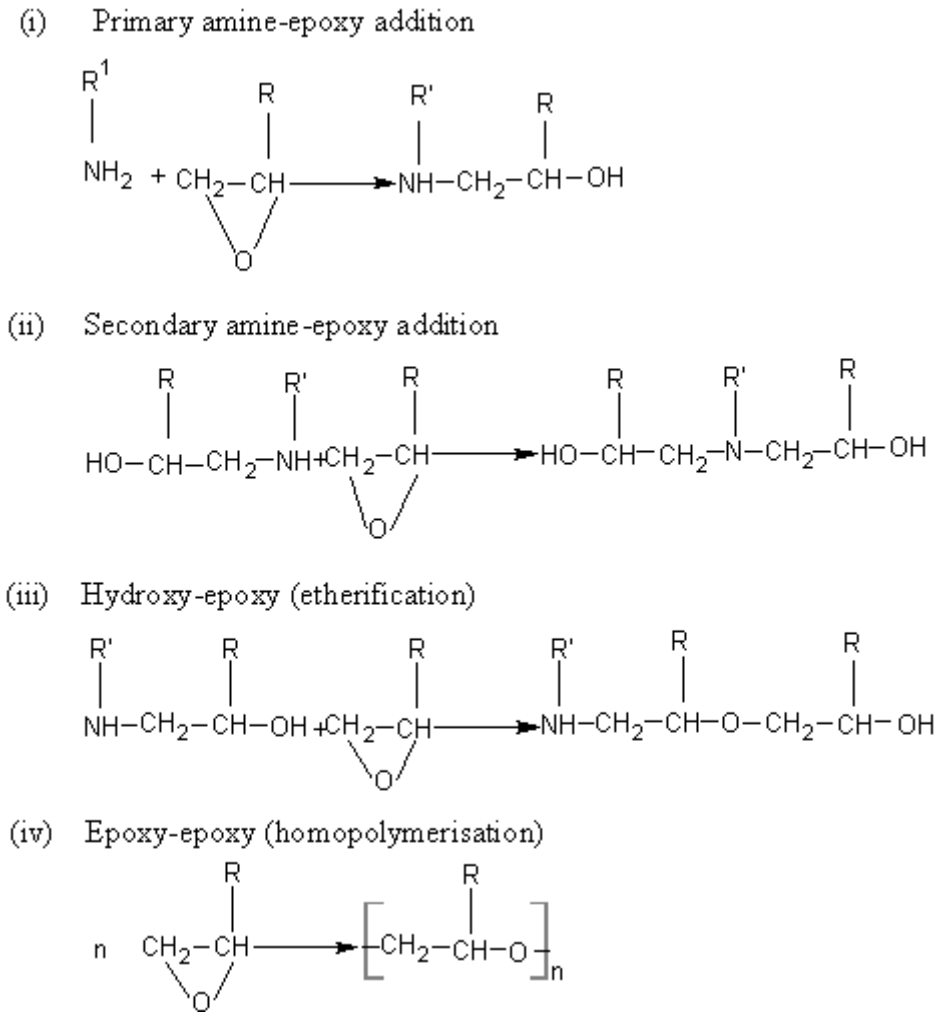

Figure 2.8: Generalised reaction scheme for an epoxy/amine resin system [38].

2.4 Optical Fibre Sensors

An optical fibre is typically a strand of glass fibre which acts as waveguides for transmitting optical signals. It consists of a core, which is of high refractive index surrounded by a lower refractive index cladding (Figure 2.9). Light transmission through the optical fibre is based on the principle of total internal reflection [39].

The increased use of advanced composites has dictated the need for new damage detection techniques for the monitoring of the structural integrity of components during their service

lives. Optical fibres have been employed as real-time damage detection tools in a wide range of application including advanced aircraft and space vehicles [40].

Optical fibre sensors can be used to measure physical parameters such as strain, temperature, pressure, velocity and acceleration, sound, state of cure, surface condition, vibration, and viscosity [41], [37], [42].

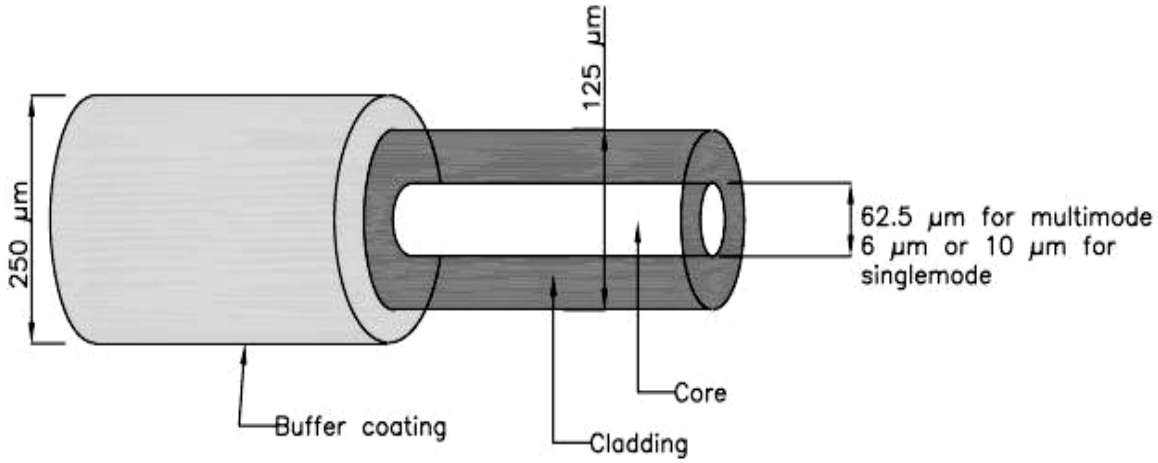

Figure 2.9: Schematic illustration of an optical fibre showing the different key components [36].

Optical fibre technology and applications have progressed rapidly in recent years. This rapidly growing interest in optical fibre-based sensing is in part due to some attractive advantages over the conventional instrumentation; for example, small size, light weight, immunity to electromagnetic interference (EMI), passive (all-dielectric) composition, high temperature performance, large bandwidth, high sensitivity, environmental ruggedness and the capability for distributed sensing. The advantages of optical fibre sensors in contrast to conventional electrical ones make them popular in different applications and currently, they are considered to be a key component in improving industrial processes, quality control

systems, medical diagnostics and preventing and controlling general process abnormalities [43].

There are various methods used in optic fibre sensing and these are based on some of the properties of optical radiation (i.e. intensity, phase, frequency and polarization, which may be modulated by the measurand [42].

2.4.1 Structural health monitoring

A structural health monitoring system for composites using optical fibre sensors is an important development in smart materials and structures. The concept of a structural health monitor uses a built-in structural diagnostic system, which were made up of three main components: actuator/sensor network, supporting electronic hardware, and data interpretation software to monitor the 'health' condition of in-service structure. The most important step of building a structural diagnostic system is the proper integration of the sensors with the structure. Optical fibre sensors are frequently embedded in composite structures as a sensor network because of their capability for distributed and multiplexed operation and high sensitivity and dynamic range. But it is difficult to embed a network of distributed optical fibre sensors in a smart composite structure as several issues in manufacturing need to be addressed.

Inorganic optical fibres and their sensors tend to be brittle and hence adequate protection must be provided when they are being integrated into the preform and used for process monitoring. In addition, exposed silica fibres are susceptible to hydrolytic degradation. Since embedded optical fibre is easily damaged in harsh environments, particularly *in-situ* during construction or fresh concrete placement. The coating materials of the fibre easily

crinkle, peel-off and generate several micro-cracks when they are embedded into cement mortar. Therefore, a new sensor based on the fibre optic technology or fabricating protection unit would be needed.

With reference to optical fibres, the protection generally takes the form of a polymeric coating (acrylate, polyamide, and fluoro-hydrocarbon). Where additional protection is required, reinforcing fibres are used in conjunction with polymeric jacketing. Protecting the sensing region is more problematic as it is important to ensure that the sensing region is not insulated or isolated from the measurand [36].

For example, Yuan *et al*. [44] recently developed a new type of sensor named a fibre-optic pre-embedded concrete bar (PECB) sensor. The technique is pre-embedding a tiny optical fibre into a matrix made from epoxy or cement based materials to form a bar. The surface of the PECB is designed in a corrugated pattern in order to improve the bonding properties between the PECB and the host concrete materials [44].

Also, optical fibres can be fitted in position depending on the type of sensor, structures where it is to be fitted and envisaged timing of fitting into the structure. For example, the surface-mountable sensor protection systems (SSPS) have been developed for fitting into an ageing (existing) engineering structure. This system uses the existing techniques and procedures that have been developed for surface mounting electrical resistance strain gauges. Typical examples were reported by Leng *et al.* [45] as a result of their research work.

Pan *et al.* [46] opined that the most effective method of preparing optical fibre sensors for embedment is to integrate the network of sensors with polyamide film as a layer, called the

optical fibre sensor layer. This layer with optical fibre sensors in it will then be embedded in the composite material.

To avoid damage of the fibre sensor during handling and moulding processes, a special supporting fixture for aligning and reinforcing the sensor is introduced. Thin and tough nylon string was used to align and guide the optical fibre in line parallel to the load direction. Both ends of the sensor were stuck on the string by using epoxy adhesive [40].

2.5 Recent Development in Self-sensing Composites

The detection of damage in fibre-reinforced composite continues to draw attention on a global scale as its interest and investment soars in recent years. But there are conventional techniques available for non-destructive testing of composite structures. These include: C-scanning, acoustic emission monitoring, x-ray radiography and thermography. Although, these techniques are well established, they are not generally convenient to be carried out on site because of the specialized equipment and expertise needed. An emerging technique is the use of fibre optic sensors for structural integrity and damage monitoring of fibre reinforced composites [11], [10]. However, as highlighted in the introduction, there are some fundamental problems with the use of fibre optic technique due to the disparity between the sizes of optical fibre (125 μm–230 μm) and that of the reinforcing fibre (7 μm–12 μm). Two of the prominent problems that may affect the damage detection and the structural integrity monitoring of composites are:

(i) the relative orientation and alignment of the optical fibre sensor in relation to the reinforcing fibres; and

(ii) The strain measurement by the sensor, which always depend on its relative location with respect to the location of the damage in the composite.

The latter may be overcome to some extent by employing multiplexing sensors but as this cannot cover the whole area of the structure; a novel idea that had been developed to extinguish these limitations is “self sensing” fibre-reinforced composites. The self-sensing composites refers to glass reinforcing composites where part of its reinforcing fibres are converted to light guides and used as sensors [8].

Reinforcing fibres have been employed as light guides in order to act in self-sensing manner, capable of detecting impact damage as low as 2 J for impacts carried out using a 20 mm hemispherical tup. Coated quartz fibres have been used instead because conventional E-glass fibres are said to be unsuitable to transmit light over long distances. The quartz reinforcing fibres have a low dielectric constant, offer high heat resistance, high resistance to thermal shock and are also commercially available. The self-sensing fibres proved more sensitive to impact damage than the conventional optical fibres used [8]. A 2 J impact event was detected successfully with reinforced fibre light guides (RFLGs) embedded in the middle of 16-ply carbon fibre composites, which represent a significant improvement over the 6 J typically obtained by the fibre fracture based sensors using standard 125 μm optical communication fibres [24].

Elsewhere, conventional sensors and techniques for real-time process monitoring of composites were replaced with E-glass fibre. This was achieved by using E-glass fibres as chemical sensors based on their ability to transmit light. This therefore provides the opportunity to monitoring light transmission intensity through the fibres during the cross-linking process.

The concept adopted for this experiment by Kister *et al.* [11] involves using cladding materials such as air, water, silicone oil, and silicone resin. Their refractive indices were lower than that of the E-glass fibres (1.56 at 23 ^{0}C and 589.3 nm). The reinforcing E-glass fibres were immersed in the various fluids and heated up to 76 ^{0}C. It was also observed that there was an increase in the light transmission through the fibres immersed in the different cladding materials as the temperature increases. Since the light transmission of the fibres increased with the temperature alone, the values of the transmission light intensity through the fibres "coated" with water, silicone oil and silicone resin were normalised with respect to the initial light intensity and also to the corresponding values of the fibres in air.

The variation of the light transmission through the E-glass fibres was explained to be due to the variation of the refractive index of the claddings as a function of the temperature. As expected, the refractive index of water, silicone oil and silicone resin was found to be decrease with the increase in temperature. This leads to an increase in the light transmission through the E-glass fibres whereas; the transmission light through the optical fibres used as a control in this experiment remained constant. Having demonstrated that the light intensity of E-glass fibre can be influenced by the variation of refractive index, an investigation was carried out to demonstrate the use of these fibres as sensors for cure monitoring.

In concluding their findings, they reported that E-glass might be used as sensors for cure monitoring based on their light transmission capability. In addition to this, an improvement in the light transmission in relation to the variation of the refractive index of the environment was observed [11].

It has been demonstrated that coating fibre bundles with appropriate cladding material improves the light transmission intensity of E-glass fibres waveguides. Three classes of

cladding materials that were evaluated are epoxy, polyurethane and sol-gel. The light transmission characteristics through E-glass waveguides was evaluated and compared. The epoxy and polyurethane cladding were found to be superior compared to sol-gel coated fibres in terms of coating quality and light transmission over specified lengths. Having achieved this, it was suggested that low-cost light sources and detectors could be used to determine if the reinforcing fibres have sustained damages or have fractured [47].

Kister *et al.* [47] also perceived that damage detection in fibre reinforced composites (FRCs) can be vision-based, for example, based on bleeding light emanating from the damage surface or where the measurand of interest can bring about a colour change in the reinforcing fibre light guide. E-glass was chosen because it's cheaper than quartz and widely used for load-bearing composites by a number of industrial sectors such as aerospace, marine, automotive and recreation.

Wang et *al.* [48] reported that two sol-gel-based compositions were evaluated and found suitable to serve as the cladding for E-glass fibres. This approach enables E-glass to be use as light guides for subsequent deployment as sensor devices for process and health monitoring. The compositions investigated were polyvinyl alcohol (PVA)-SiO2 and GLYMO-SiO2 because they were chemically similar in composition to that used as the coupling or sizing agent in E-glass fibres (i.e. organo-silanes).

Wang [48] also reiterated that the application of organo-silanes in the generic area of sol-gel based materials is well established. Therefore, sol-gel has been found to be suitable for optical applications as it enables good control of the composition and the general properties of the final materials. There is however, a major concern with the deployment of sol-gel based material. This is the formation of shrinkage-induced cracks during the densification

process. This is because material experiences relatively large volume shrinkage as a consequence of loss of solvent and small-molecular weight by-product of hydrolysis and polycondensation such as water and alcohol. In order to obtain crack free coatings, they claimed to have used two different methods based on conventional sol-gel processing. The first method was using tetraethoxysilane (TEOS) and polyvinyl alcohol as precursors (the structure is as illustrated in Figures 2.10 (a and b) while the mixtures of acid-catalysed solutions of TEOS with 3-glycidoxypropyltrimethoxysilane were used as precursors. UV-visible transmission results showed that the films had low absorption and high transparency in the visible range. The refractive indices of the films were found to be a function of the molar fractions of the major chemical components. And when the light transmission characteristics of the coated fibres and their mechanical properties were evaluated, the sol-gel coatings were found to be more effective in converting the conventional E-glass into light guides.

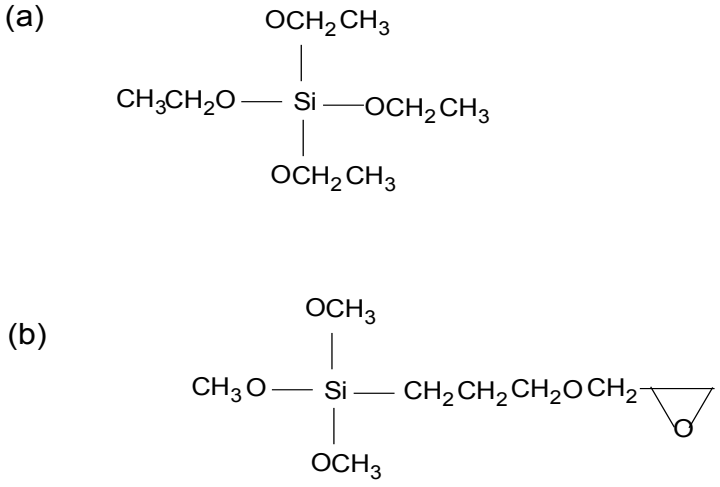

Figure 2.10: Structure of precursors: (a) TEOS (b) GLYMO [48].

It was also reported in another studies that the macroscopic failure of the "mini-composite" could be tracked by monitoring the transmitted light intensity through the fibres as a

function of the applied stress. The images captured with a CCD-camera were eventually used to determine the attenuation of the light intensity and also obtain information on the fibre fractures over the cross-section of the bundle [49].

Kister *et al.* [49], reported on the conversion of conventional reinforcing E-glass fibres into light guides by using polyurethane or epoxy-based resin as cladding. These reinforcing fibre light guides (RFLGs) were either surface mounted or embedded on/in glass fibre reinforced polymer (GFRP) composites. These RFLGs were used as sensors to detect damages unleashed on the structural component by the actions of impact, indentation and flexural loadings. The presence of the damages was detected successfully by monitoring the transmission characteristics through the RFLGs. The study concluded that:

(i) the light transmission of the light guides was attenuated after impacting the self-sensing composites at 2 and 10 J. Although, an increase in impact energy causes a significantly larger delamination area, the light transmission was only reduced slightly due to the fact that the diameter of the hemispherical impacter was much larger than the width of the self-sensing fibres;

(ii) also, increase in indentation loading causes attenuation of the light transmission through the RFLGs. Part of the attenuation was recovered when the load was removed. A CCD camera was used to record variation in the light intensity during the indentation test;

(iii) as the flexural loading (three-point bending) increases, the light transmission of the RFLGs was continuously attenuated. When the flexural tests were conducted to failure of the specimen, there was no recovery of the light transmission sighted after unloading; and

(iv) the damaged area on the self-sensing composites was located by means of the bleeding light emanating from the damaged RFLGs [49].

In the study by Fernando and Degamber [36], the possibility of using E-glass fibre for cure monitoring was demonstrated. In this study resins was used to impregnate E-glass using evanescent waves where the spectra obtained showed the depletion of the amine and the epoxy functional groups as a function of processing at 80 ^{0}C. The refractive index of the bulk E-glass was found to be greater than that of the resin or cladding at cross-linking, which therefore mean that E-glass can act as optical waveguides [36].

Although the above-mentioned papers demonstrated the concept, real-time damage detection was not demonstrated and furthermore, the fabrication of void-free self-sensing composites was not developed or demonstrated. Moreover, none of the existing literature reported monitoring of the resins height during fibre impregnation whilst composite is being manufactured. Another unique achievement being proposed here is to monitor the cross-linking process of the composite in real-time inside the oven using 1 m of small-diameter optical fibre (SDOF).

Chapter 3

Experimental Setups & Procedures

3.0 Introduction

A number of experiments were carried out to fulfil the aims and objectives mentioned in Chapter 1. This called for the preparation of a number of different fibre bundles and composites of specified dimensions. These samples were used for characterising the transmitted light intensity, temperature, impregnation of the fibres, cure behaviour and tensile properties.

3.1 Materials

PPG Industries, UK, supplied the continuous water-sized E-glass fibres used in this project. Each fibre bundle contained 2400 individual filaments. In addition to E-glass, custom-made small-diameter optical fibres from Schott-Glass were also used. The resin systems used were EPO-TEK® 314 (supplied by Dow Corning, U.K.) & 310M (supplied by Dow Corning, U.K.). The EPO-TEK® 314 resin system was used for mechanical tests and the EPO-TEK® 310M was used for *in-situ* process monitoring. Other equipment and components employed were:

(i) SMA connector (supplied by Thorlabs, U.K.) for potting the fibre bundle prior to polishing;

(ii) rectangular glass moulds;

(iii) syringes (supplied by Thorlabs, U.K.) for injecting resins into the mould;

(iv) Freekote-700 (supplied by Aerovac, U.K.) was used as release agent for easy de-moulding of composite after curing; and

(v) a power-meter to monitor the transmission light intensity of fibre-reinforcements during process monitoring.

3.2 Characterising the As-Received Small Diameter Optical Fibre

A few filaments of the SDOF were cut and fixed on an aluminium stub and then gold-coated (using SC500 manufactured by Emscope, U.K.) in preparation for scanning electron microscopy (SEM).

3.2.1 SMA connectors

In order to couple light into the SDOF bundle, it was necessary to attach standard sub-miniature adapter (SMA) connectors into the ends of fibre bundle prior to polishing. This was carried out by potting each fibre bundle ends into the adapter (SMA) connector. An automatic polishing unit was used to polish the end-faces of the potted fibre bundles.

3.2.2 Binder removal

The binders on the SDOF were removed by pyrolysis. The optimum pyrolysis temperature and duration combination were obtained by trial-and-error. The optimum pyrolysis temperature was found to be 450 ^{0}C. The pyrolysis experiments were carried out on 1 m length SDOF for 4, 6, 8, and 10 hours. The samples that were pyrolysed at 450 ^{0}C for 6 hours yielded clean surfaces as inferred via SEM analysis.

3.2.3 Etching of small diameter optical fibre

Etching of the SDOF using hydrofluoric acid (2.5 %) was an additional procedure carried out on SDOF after pyrolysis to reduce the diameter of the cladding. This was done to access the evanescent field when the SDOF was illuminated. These fibre bundles were etched to 60 %, 70 %, 80 % and 90 % of their original light transmission intensity. The sample used for this study was etched with 2.5 % of hydrofluoric acid and 97.5 % of distilled water.

A procedure was developed to monitor the transmitted light intensity during the etching process. Here, both ends of the fibre were potted into the SMA connector and polished as discussed previously. One end was then connected to the halogen light source (HL-2000-HP-FHSA manufactured by Mikropack) whilst the other end was connected to one end of the optical power meter (supplied by Thorlabs, UK). A schematic illustration of the experimental setup for the etching experiments is shown in Figure 3.1. The optical power meter was connected to a computer system from which the light intensity data were acquired through the use of PM100 Labview software.

Two regions, as illustrated in Figure 3.1, were sealed with wax (approximately 5 cm from the centre to either side of the sample) to contain the HF acid whilst monitoring the light through the fibre bundle. The transmitting light intensity monitored via the optical power meter was used to control the etching time. Once the desired light transmission through the SDOF was achieved, the sample was removed from the etching solution and rinsed with distilled water before being oven dried at 40 ^{0}C for 3 hours. The etched fibre bundles were subsequently used for cure monitoring experiments

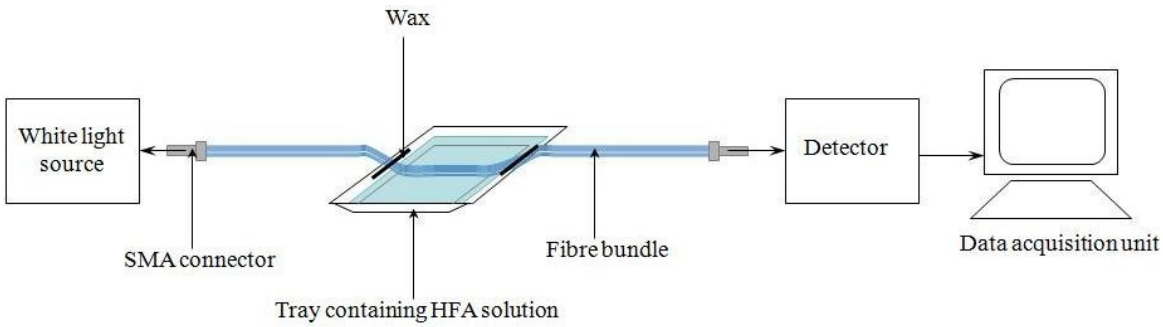

Figure 3.1: Schematic illustration of the experimental set-up for etching SDOF.

3.3 Fabrication of Tensile Test Specimens

3.3.1 Fabrication of fibre bundles

The gauge length of the specimen was 100 mm. The total length of fibre bundles specimens fabricated from E-glass and SDOF was 280 mm. Tensile test specimens were produced from water-sized E-glass and SDOF bundles. Custom-designed end-tabs (Figure 3.2) were used to fabricate E-glass and small-diameter optical fibre bundles for tensile testing. A photograph of a fabricated fibre bundle is presented in Figure 3.3. The two free-ends of the fibres were potted into the SMA connector then polished to facilitate coupling of a white/laser light source to one end whilst the opposite end was used to capture images via a high speed CCD camera. Scotch-weld 9323 adhesive (supplied by 3M, U.K.) was used to secure the fibre bundle between the end-tabs. Adequate care was taken to ensure even tension of individual fibre filaments but this could not be guaranteed due to the number of filaments in the bundle (approximately 2,400 and 2,800 for E-glass and SDOF respectively).

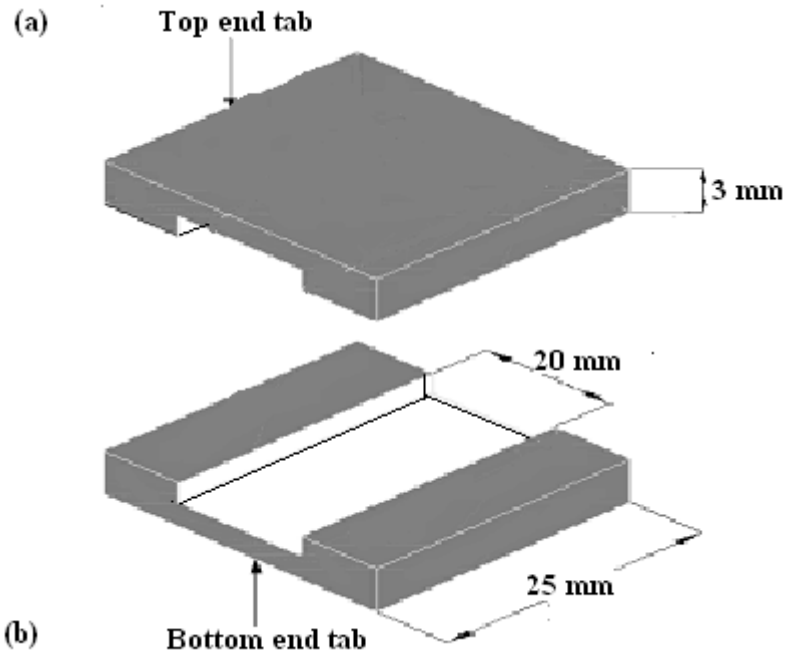

Figure 3.2: Schematic illustration of end-tabs with grooves to accommodate fibre bundles. The pair include (a) for top and (b) bottom respectively.

A photograph of a fibre bundle with SMA connectors and end-tabs is shown in Figure 3.3.

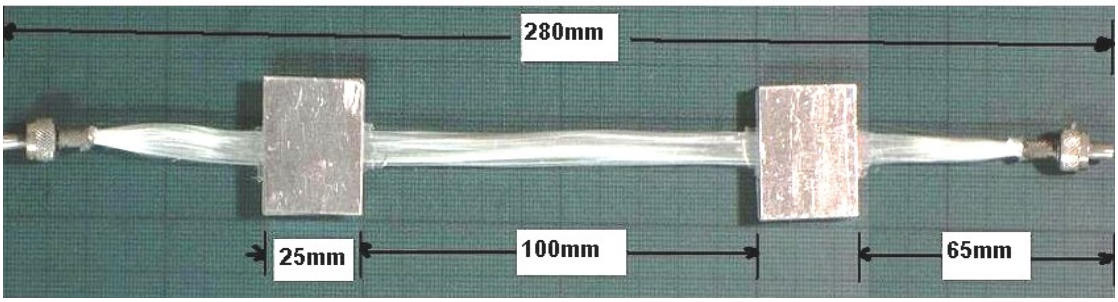

Figure 3.3: Photograph of a fibre bundle sample with end-tabs and SMA connectors.

3.3.2 Fabrication of composites

The most effective technique for fabricating void-free composite specimens was established by trial-and-error. This selected method was achieved by sandwiching reinforcing fibres between two glass plates (supplied by Artic Glass & Glazing Company

Limited, U.K.). The top and bottom plates were 150 mm and 300mm in length respectively; both plates were 30 mm wide and 6 mm thick.

Two rectangular moulds were formed by securing strips of adhesive PTFE release-film (supplied by Aerovac, UK) to each plate; schematic illustration of glass mould is shown in Figure 3.4. These moulds served to contain the resin, and had cavity dimensions of 150 mm (length), 25 mm (width) and 0.5 mm (depth).

A release agent, Freekote-700 (Aerovac, UK), was applied to the glass plates before assembly to allow for easy de-moulding of the composite after curing. The fibres were secured in position on the bottom plate before the top plate and mould was aligned. Two needle-attached syringes were positioned in opposite directions to each other within the mould and secured using RTV 3140 silicone resin (supplied by Dow Corning, U.K.). The glass plates were clamped in place and sealed using silicone resin.

A photograph of a composite tensile test specimen with SMA connectors and end-tabs is shown in Figure 3.5.

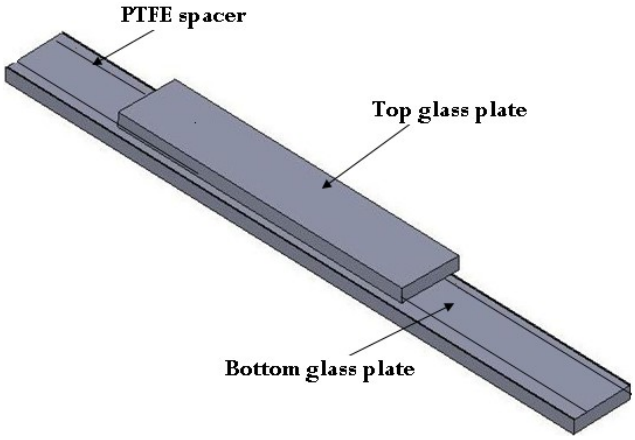

(i) Schematic illustration of a complete mould showing PTFE spacers.

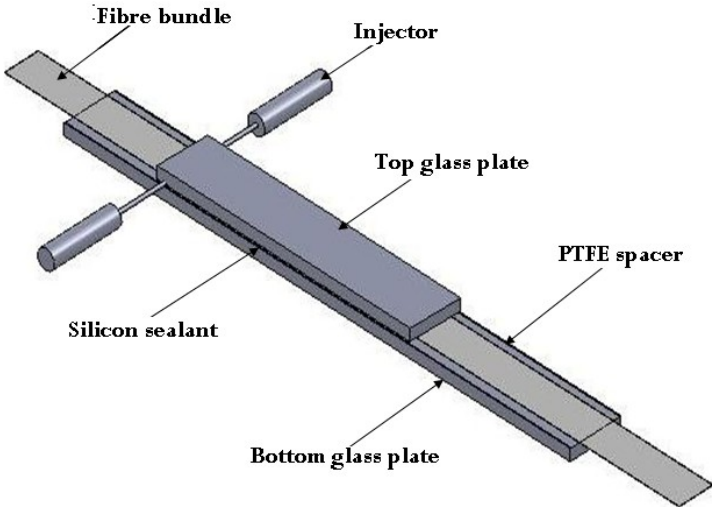

(ii) Schematic illustration of an assembled mould.

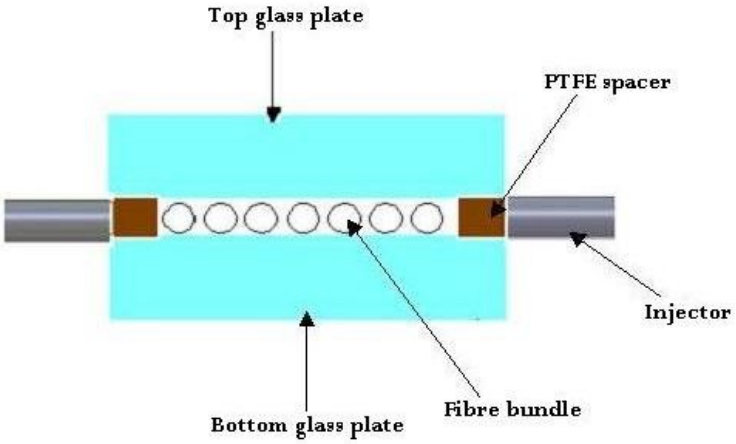

(iii) Cross sectional view of an assembled mould.

Figure 3.4: Schematic view of the fabricated composite glass mould and composite manufacturing process: (i) 3-D view of a complete mould; (ii) 3-D view of the assembled moulds showing PTFE spacers, fibres bundle, injector with silicone sealant; and (iii) Cross-sectional view of the assembled moulds.

The fibres between the SMA connectors and the end-tabs were not impregnated because it was necessary to bend these sections out of the jaw of the mechanical test machine. As stated previously, one of the SMA connectors was connected to the light source and the other end was linked to a high-speed CCD camera.

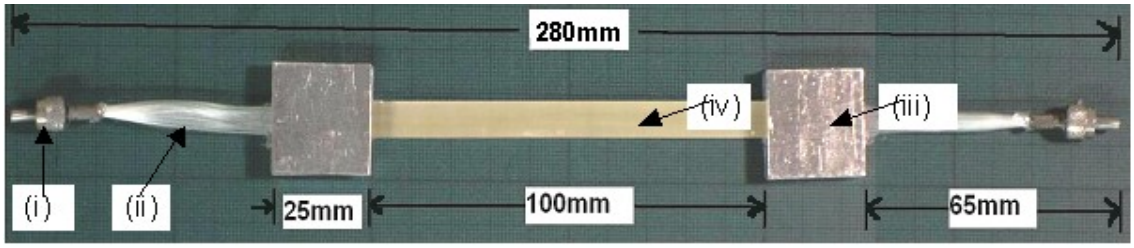

Figure 3.5: Photograph of an E-glass composite sample with SMA connectors and end-tabs: (i) SMA connector; (ii) Un-impregnated section of the E-glass fibre bundle; (iii) End-tab; (iv) Void-free composite.

3.3.2.1 Fibre impregnation and cross-linking

A two-component resins system; EPO-TEK® 314 was prepared and used for the impregnation studies. Fresh batches of resin and hardener were weighed using a stoichiometric ratio of 100:6 (epoxy: amine), mixed thoroughly, and then degassed in a vacuum chamber for 30 minutes.

The assembled glass mould with the fibre bundle was placed vertically and the EPO-TEK® resin system was injected into the mould via two syringes either manually or by using automated pumping systems as illustrated in Figure 3.6. Once completed, the syringes were detached and needle holes sealed using silicone resin. The set-up was placed in an air-circulating oven and the resin system underwent cross-linking at 120 °C for 3 hours. After cooling to room temperature, the composite was de-moulded.

As the mould was larger than the width of the reinforcing fibres, it was necessary to polish the excess resin down the length of the specimen. Un-impregnated fibre-ends were then potted into SMA connectors and polished appropriately while end-tabs were attached to the un-impregnated fibre section using the methods previously illustrated here. A photograph of one of the composite samples prepared for tensile test is shown in Figure 3.5.

Figure 3.6: Experimental setup – impregnation of E-glass (**a.** Automated syringe driver; **b.** Laser light source; **c.** Power meter; **d.** Calibrated unit; **e.** Assembled composite moulds with fibre bundle ready for impregnation; and **f.** Injector).

3.4 Fabrication of Test Specimen for Process Monitoring

The moulds used for this experiment is the same as the schematic illustration presented in Figure 3.4. The sample preparation was carried out as described previously for the composites earlier in Section 3.3.2.1.

The setup used for the on-line process monitoring experiments is illustrated schematically in Figure 3.7. The instruments were switched on for 1 hour prior to starting the experiment. The fabricated sample was placed carefully in a vertical position in a temperature-controlled oven (SDOF sample only). The two long (42.5 cm each) un-impregnated fibre ends fitted with polished SMA connectors were passed out through the door of the oven. One end was connected to the white-light source (WLS100, manufactured by Bentham Instrument Ltd., UK) and the other to one end of the optical power meter. The output of the optical power meter was connected to the data acquisition computer system loaded with PM100 Labview software. EPO-TEK® resin system was injected via two syringes into the mould in batches to allow full impregnation of the fibre length.

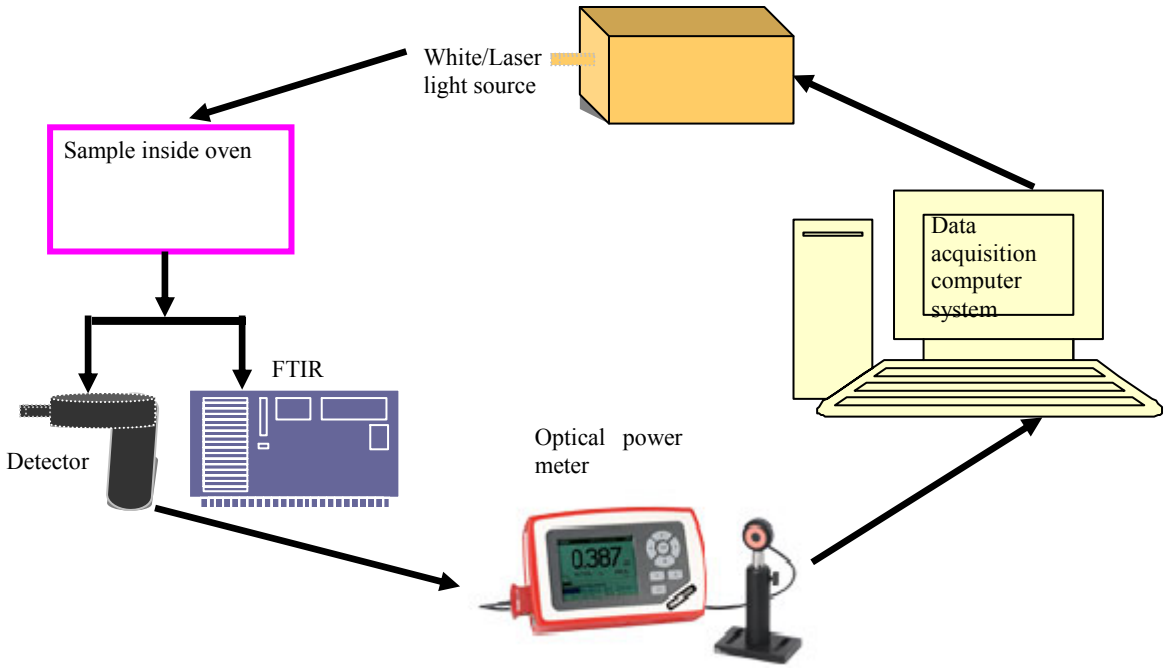

Figure 3.7: Schematic illustration of the experimental setup for monitoring the impregnation process.

Once the impregnation operation completed, the syringes were removed and the holes were sealed as described previously. The recording of data by the PM100 Labview software was

halted whilst one of the SMA connector was disconnected from the optical power meter and subsequently connected to the FTIR channel for monitoring the cross-linking reactions. The resin system was cross-linked at 65 °C for 5 hours

A water-sized E-glass sample was prepared using the same techniques employed for the SDOF sample described previously. The apparatus were setup and the experiment was carried out in a temperature-controlled room as it was:

(i) impracticable to carry out the experiment inside the oven as described for the SDOF due to shorter sample length; and

(ii) the limitation in light transmission of E-glass.

A laser light source was used to illuminate the E-glass sample and the PM100 Labview software was used for data acquisition. Two automatic resins injection units as described previously were used to fill the mould. A ruler was mounted on the mould for monitoring the impregnation rate of the fibres. After the syringes were removed as mentioned earlier, the mould was transferred to a hot-plate for initiating the monitoring and cross-linking process. The experimental setup involving the E-glass sample was similar to that illustrated in Figure 3.7 except that a hot-plate was used.

After cooling to room temperature, the composite was de-moulded. As the mould was larger than the width of the reinforcing fibres it was necessary to trim the excess resin. It was not possible to polish the composite because of its flexibility.

3.4.1 Effect of temperature on light transmission

These experiments were carried out to investigate the effect of temperature on the transmitted light intensity characteristics of small-diameter optical fibre (SDOF) bundles.

The fibre bundle with polished SMA connectors was set-up in the oven as described previously. The polished ends were connected to a power meter and a light source. The power meter was connected to the computer systems through which data were acquired using PM100 Labview software.

At the start of this experiment, the oven door was left opened for 30 minutes and thereafter closed for 1 hour in order to observe the stability of the light transmission at room temperature. When the transmitted light intensity was found to be stable at room temperature, the oven was switched on. After 3-5 minutes of observation at 22 ^{0}C temperature, the temperature was increased to 40 ^{0}C and held for an hour whilst recording the transmitted light intensity. This same procedure was repeated at 60 ^{0}C, 80 ^{0}C, 100 ^{0}C, and 120 ^{0}C for the first sample. In the case of the second sample, it was subjected to the same temperature regimes but it was heated to 150 ^{0}C and 180 ^{0}C. In both cases, the temperature was held for 1 hr at each temperature.

3.5 Mechanical Testing

3.5.1 Tensile testing of fibre bundles and composites

Mechanical tests were carried out on these samples using an Instron 5566 machine with data logging via Merlin TM software. A charged coupled device (CCD) high-speed camera (FastCAM 1024 PCI, Photron, UK) was used to image the polished end of the fibre bundle and also for monitoring the sequence of failure as the test progresses. The high-speed camera was synchronised with a conventional piezo-electric acoustic emission system (Physical Acoustics Limited, UK) and the mechanical test machine (Instron 5566). The camera was triggered when a fibre fracture was detected by an acoustic emission (AE)

transducer during mechanical loading. Two Micro-R-15 piezo-electric transducers (Physical Acoustics Limited, UK) were mounted 10 cm apart on the surface of the test specimen to record the acoustic emission. The loading was carried out at a cross-head displacement rate of 1 mm/min at room temperature.

Chapter 4

Results and Discussion

4.0 Introduction

This chapter summarises the results obtained and it presents a detailed discussion on the following topics:

(i) etching of the small-diameter optical fibre (SDOF) to reduce the thickness of the cladding;
(ii) effect of temperature on the light transmission characteristics of etched SDOF;
(iii) a feasibility study into the possibilities for monitoring the impregnation process;
(iv) demonstration of cure monitoring the etched, heat-treated and impregnated fibres; and
(v) damage detection using the SDOF and E-glass fibre bundles and composites.

4.1 Etching the Small Diameter Optical Fibres

The as-received SDOFs cladding was etched in hydrofluoric acid (HFA) to reduce the thickness of the cladding. This procedure was necessary to partially expose the evanescent field of the optical fibre. This section discusses the effect of specified concentrations of HFA on the etching rate and the transmitted light intensity during the etching process.

Figure 4.1 shows the observed trends of normalised transmitted light intensity in the SDOF as a function of time using a pre-determined concentration of hydrofluoric acid. It is evident

from Figure 4.1 that the normalised transmitted light intensity is a function of the thickness of the cladding. The rate of etching of the cladding is also influenced by the concentration of the hydrofluoric acid.

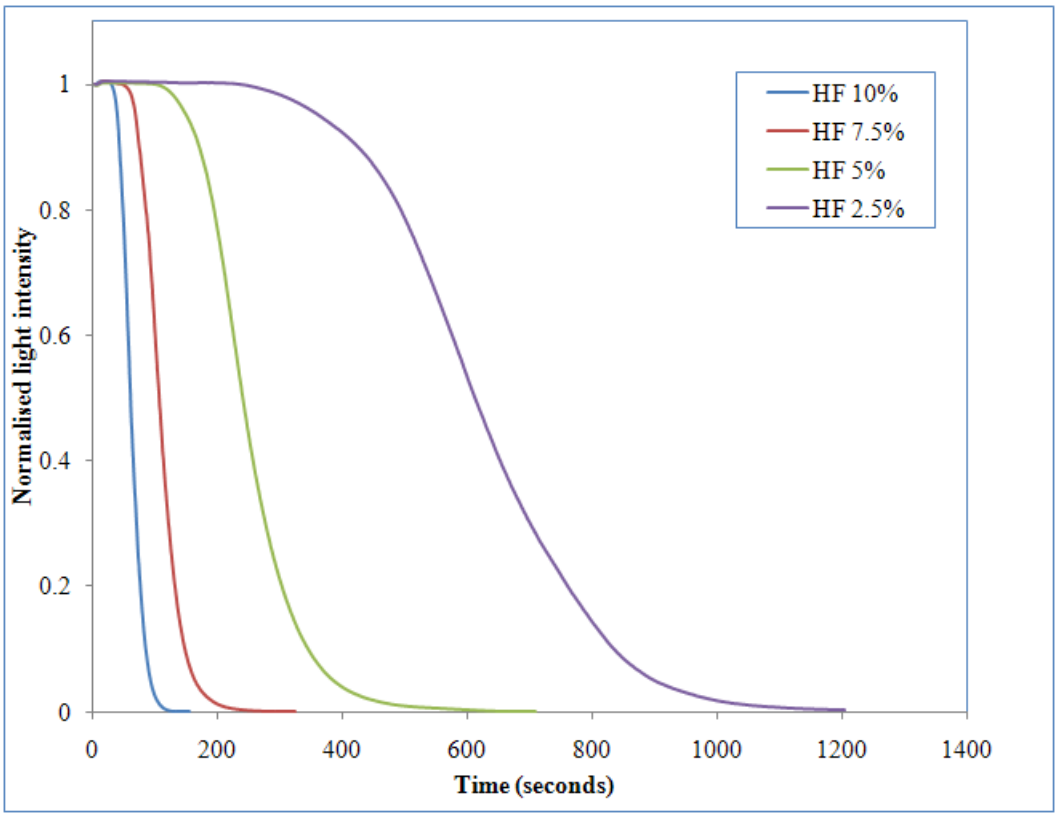

Figure 4.1: Normalised light intensity versus time graph showing the rate of etching as a function of rate of concentration of hydrofluoric acid in the etching solution. Data generated by Dr. Liwei Wang, Sensing and Composites Group.

In Figure 4.1, the onset of the attenuation of the normalised transmitted light intensity can be attributed to the dissolution of the cladding causing the evanescent field to be exposed to the HFA. These experiments were carried out at ambient temperature (23.6 ^{0}C). It is readily apparent from Figure 4.1 that the dissolution of the cladding was influenced strongly by the concentration of the HFA.

Since only authorised users were permitted to work on the HFA etching facility, the data presented in Figure 4.1 and 4.3(a) were generated by a post-doctorate research fellow on an EPSRC project. Figure 4.1 data were generated by Dr. Liwei Wang. Figure 4.2 shows the rate of etching and the onset of attenuation of the transmitted light intensity as a function of concentration of the HFA. It also shows that the rate of etching of the cladding increase exponentially with the concentration of the HFA. Likewise, it is also apparent that the time taken for the onset of attenuation of the transmitted light intensity is significantly influenced by the concentration of the HFA.

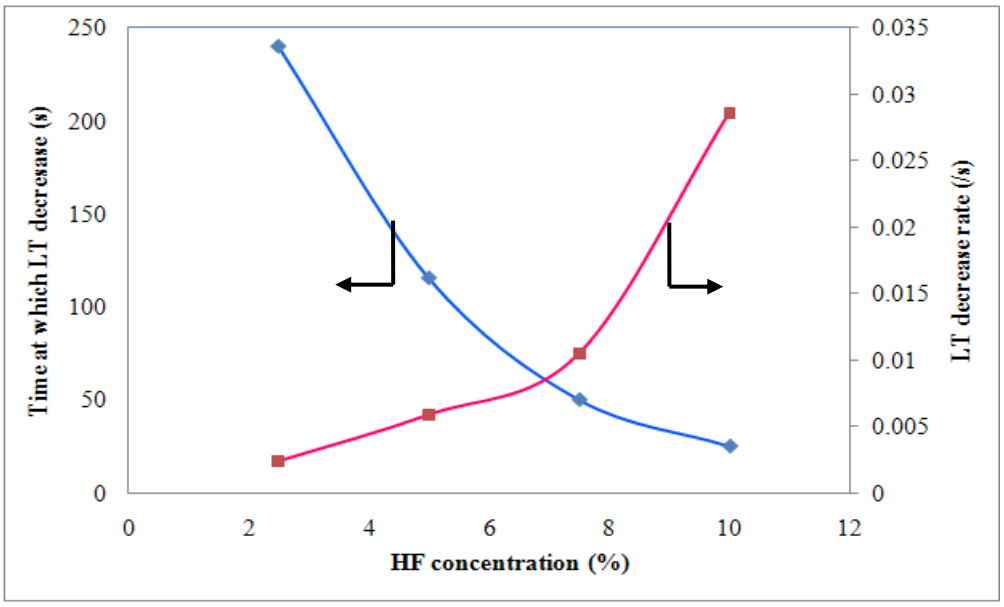

Figure 4.2: Graph showing the rate of etching and the onset of attenuation of the transmitted light intensity as a function of the concentration of HFA.

"LT" = Light transmission

It can also be seen in Figure 4.1 that the time for the onset of attenuation for the 2.5 % HFA was approximately 240 seconds. Since the 2.5 % HFA solution was available, a new SDOF bundle, 100 cm long sample, was prepared for etching. This procedure was carried out at

room temperature but the etching was terminated when the transmitted light intensity dropped by 20 % of its original value.

Figure 4.3(a) presented the data generated from the previous procedure. It can be seen that no data was recorded at initial stage of the experiment. This is due to the fact that the recording was started too earlier than the experiment. Hence, Figure 4.3(b) shows the corrected version where this stage has been manually eliminated.

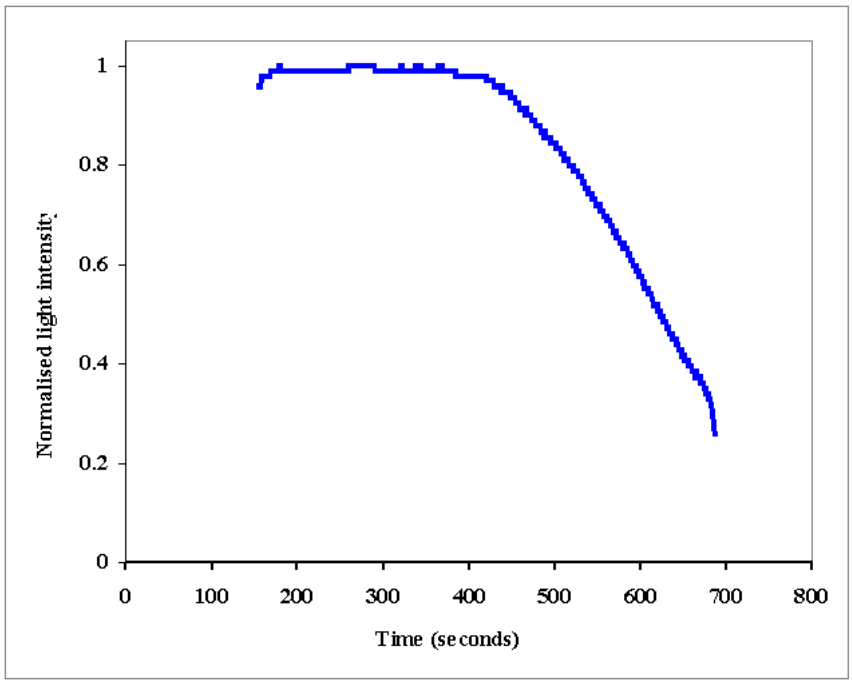

Figure 4.3(a): Graph showing changes in the normalised transmitted light intensity during etching of SDOF.

With reference to Figure 4.3(a), the horizontal section of the graph represents the initial stage of the attenuation process which was due to the etching of the cladding by the HFA solution. However, this demonstrates the presence of a significant cladding thickness since attenuation was minimal until after approximately 240 seconds when the rate of attenuation

was 0.0024. At this stage, the cladding on the SDOF was progressively etched and this can be observed in the normalised transmitted light intensity graph.

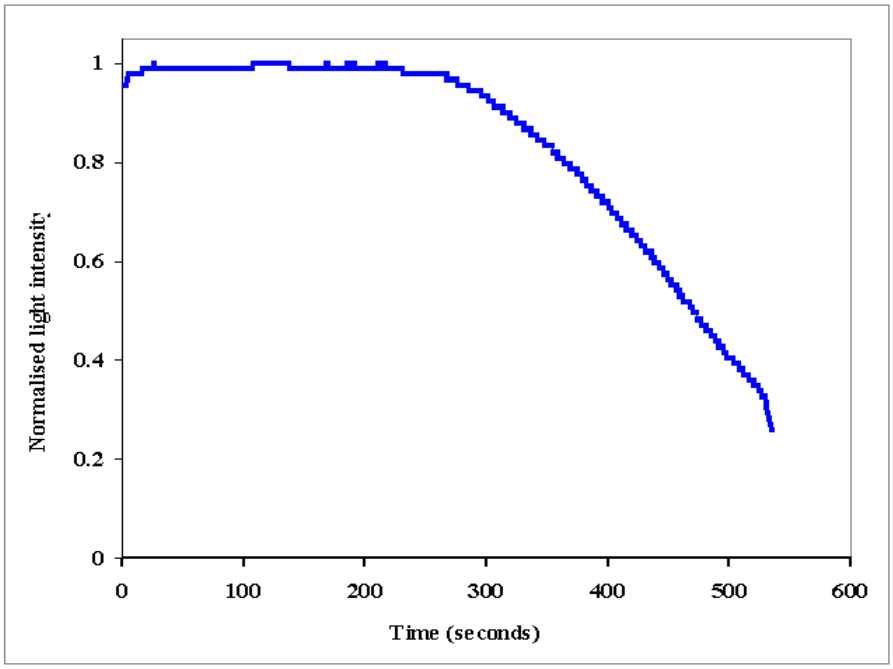

Figure 4.3(b): Manually corrected version of normalised light intensity graph during etching of SDOF shown in Figure 4.3(a).

In conclusion, it was demonstrated successfully that the SDOF could be etched in HFA to reduce the thickness of the cladding. The rate of etching was found to be influenced by the concentration of the HFA. The on-line monitoring technique developed in this study can be used to control the thickness to the desired thickness. This method can be used to produce optical fibre sensors for evanescent wave spectroscopy.

4.2 Effect of Temperature on Light Transmission Intensity

Here the effect of temperature on the light transmission characteristics through the pre-etched SDOF bundle from Section 4.1 and Figure 4.3(b) was investigated. The experimental procedure was presented in Section 3.4.1.

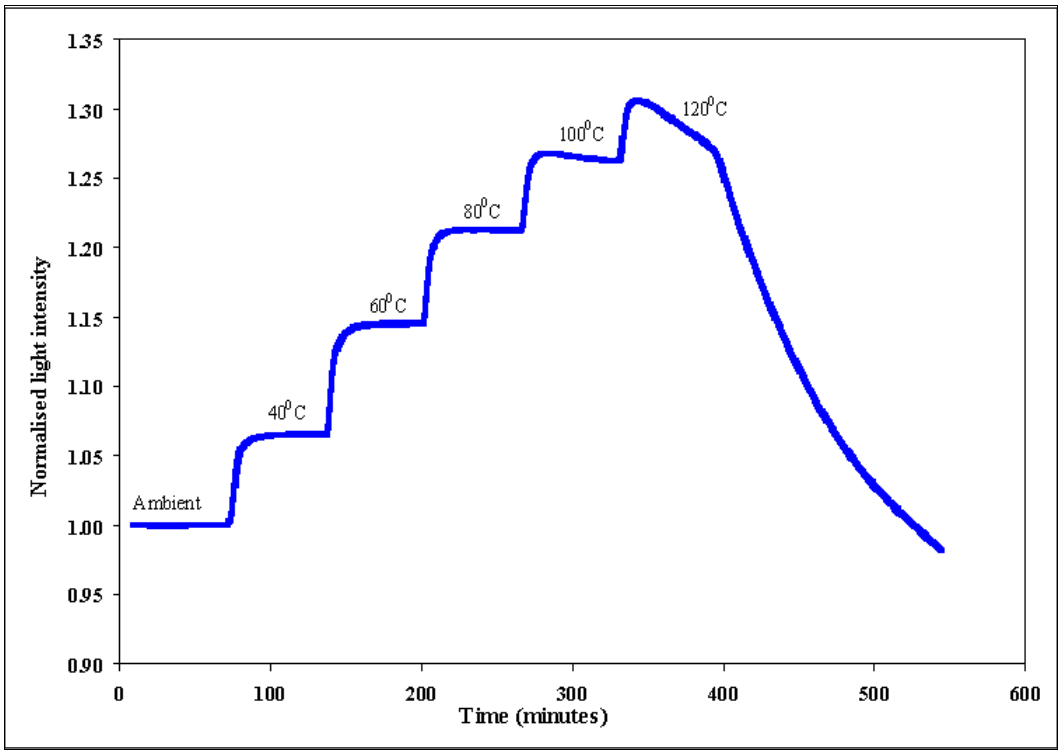

Figure 4.4(a): Graph showing changes in the transmitted light intensity during heating of pre-heat-treated and etched SDOF.

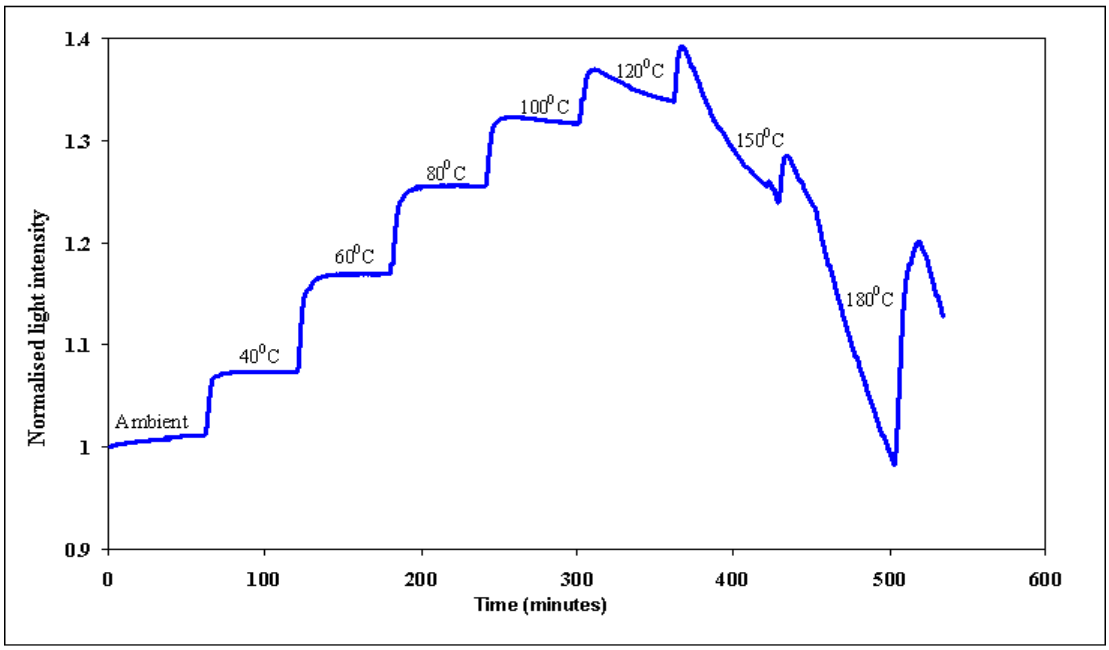

Figure 4.4(b): Graph showing changes in the transmitted light intensity during heating of pre-heat-treated and etched SDOF; This represent the second ramp/hold experiment that was carried out on the SDOF that was used in Figure 4.4(a).

Figure 4.4(a) illustrates the effect of temperature on the transmitted light intensity through the SDOF bundle. In Figure 4.4(a), it is observed that the transmitted light intensity is stable at each of the temperature 'hold' periods. However, after 120 ^{0}C, the stability of the transmitted light intensity was seen to be decreasing. At this stage, the sample was allowed to cool down to ambient temperature. Figure 4.4(b) shows the transmitted light intensity for a repeated experiment using the same fibre bundle but the final temperature was increased to 180 ^{0}C. The transmitted light intensity was stable at each of the 'hold' periods up to 100 ^{0}C before decreasing as observed in the first experiment. A possible reason for this observed decrease in the transmitted light intensity was the fact that a 'black wax' was used during the etching process to control the length of SDOF that was exposed to the acid. Since the wax was not removed for the temperature trials, above its melting point, it could have flowed along the SDOF via capillary action. This assumption is supported by the repeat-experiment that was carried out on the same sample of SDOF bundle where the transmitted light intensity was observed to have been decreased in a similar way to the first attempt after approximately 100 ^{0}C.

In order to investigate this, a fresh SDOF bundle was prepared by potting SMA connectors to both sides and polished whilst the temperature ramp/hold experiments were repeated. However, the black wax was not used during the etching process.

Figure 4.5 shows that the attenuation in the transmitted light intensity did not decrease after 100 ^{0}C as observed in the previous two trials. The experiment was therefore terminated at 180 ^{0}C and the sample was allowed to cool to ambient.

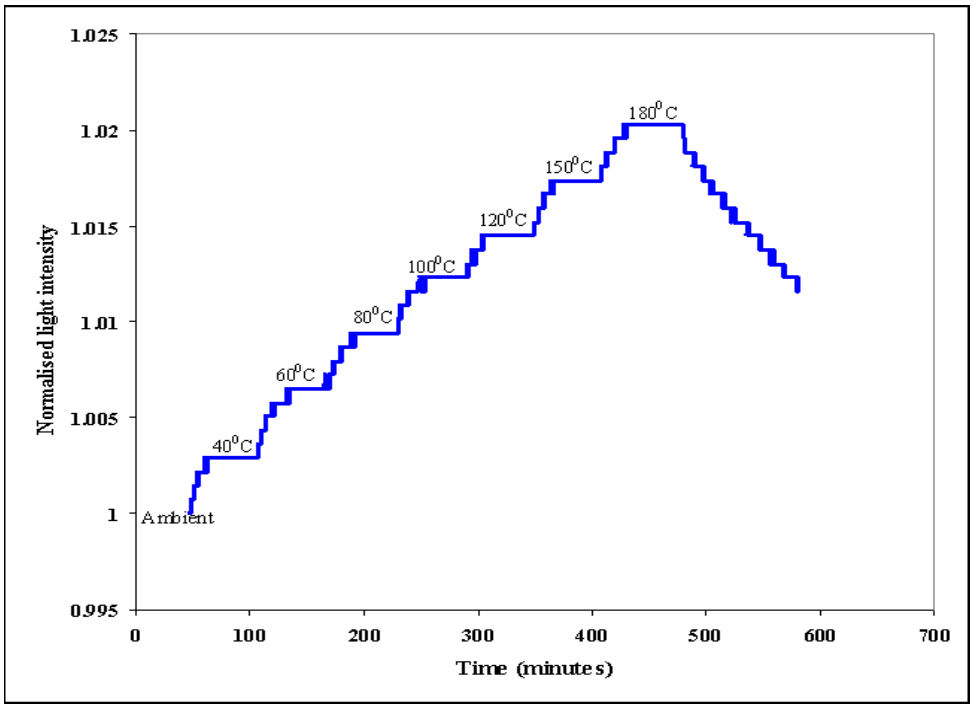

Figure 4.5: Graph showing changes in the normalised transmitted light intensity during heating of pre-heat-treated and etched SDOF where wax was not used.

In conclusion, it was demonstrated successfully that the SDOF can be used as intensity-based sensor for monitoring the temperature. It is proposed that the SDOFs can be used whilst processing to indicate the temperature of the reinforcing fibres. This will obviously negate the need for thermocouple to be inserted into the preforms.

4.3 Characteristics of *in-situ* impregnation and cure monitoring of fibre bundles

The mode of operation of a conventional optical fibre relies on total internal reflection. The key characteristic of an optical fibre are its circular cross-section, the core and the cladding where the refractive index of the core is higher than that of the cladding. E-glass fibre can act as waveguides if cladding (matrix) can be introduced around the fibre ensuring that the conditions of total internal reflection are maintained. The same applies to the SDOF used in this study. However, in this instance the core was surrounded by a silica cladding. In the self-sensing composite, the matrix acted as the cladding.

However, with reference to chemical monitoring, it is necessary to access the evanescent field in these fibres. With the small diameter optical fibres that were available, cladding had to be etched to access the evanescent field. When an absorbing media is present in the cladding, this component will be absorbed when inspecting the transmitted light characteristics. For example in the current case, functional groups such as the amine, the epoxy and the C-H will be absorbed in the near-infrared. Therefore, by analyzing the output spectrum of the transmitted light, the contribution from the absorbing media can be deduced. Thus, evanescent wave spectra can be used to monitor the impregnation and curing processes.

4.4 Impregnation Monitoring of SDOF

The current series of experiments were carried out using a 100 cm length of SDOF bundle prepared, as described in Section 3.3.2.1, for monitoring impregnation in real-time.

A light source was connected to one end of a potted and polished SMA connector whilst the other end was attached to a detector (an optical power meter) where the light intensity was monitored.

The resin system (mixed resin and hardener) was injected manually into the mould (see Section 3.3.2.1) for details of the experimental set-up.

In Figure 4.6(a), the points designated ‘A’, ’B’, ’C’,.....,’K’ represent the case where the resins was injected manually into the mould via a syringe. As the resin was injected manually, it was not possible to control the volume of resin that was dispensed. With reference to Figure 4.6(a), the initial attenuation at point ‘A’ represents the core where EPO-TEK® 310M (with RI=1.4) comes into contact with the pre-etched SDOF. The

significant drop experienced by the normalised transmitted light intensity at point E was due to injection of a larger volume of resin than desired into the mould; the same applies to points F and G. However, the uncontrolled resin injection into the mould does not detract from the desired outcome; because this experiment has shown that the evanescent field in the optical fibre can be accessed to monitor the impregnation process in real-time.

The data-set displayed in Figure 4.6(b) is identical to that presented in Figure 4.6(a) except that the sudden drop in the normalised transmitted light intensity between A and K have been removed manually (intentionally). It is emphasised that spurious points were removed intentionally.

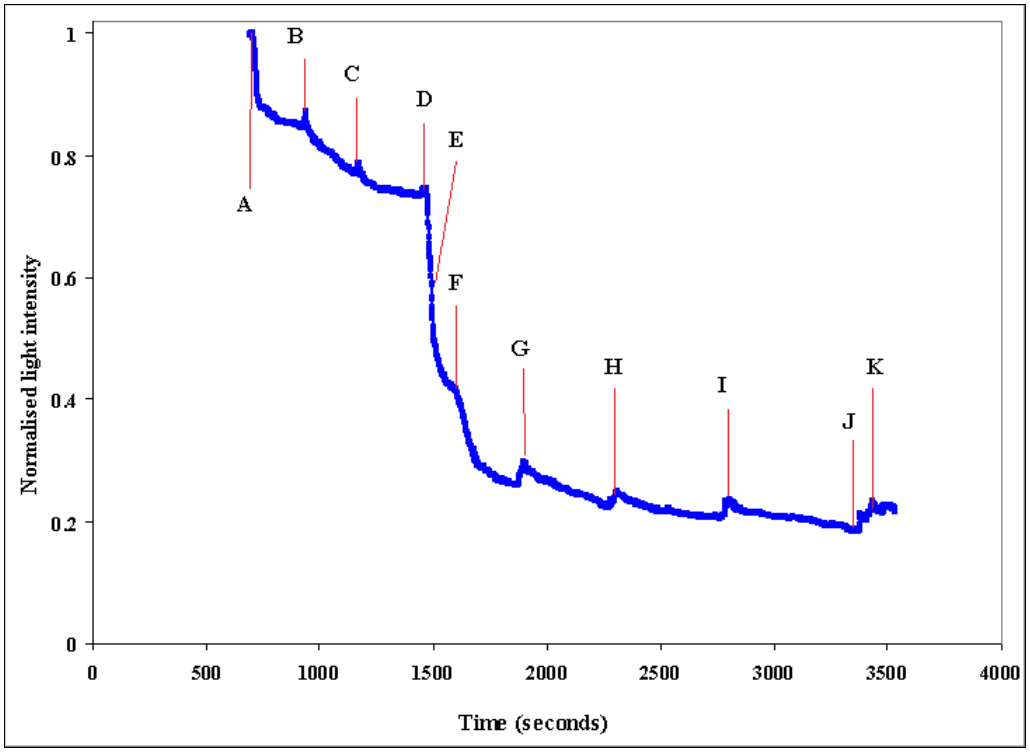

Figure 4.6(a): Graph showing changes in the normalised transmitted light intensity during impregnation of pre-heat-treated and etched SDOF.

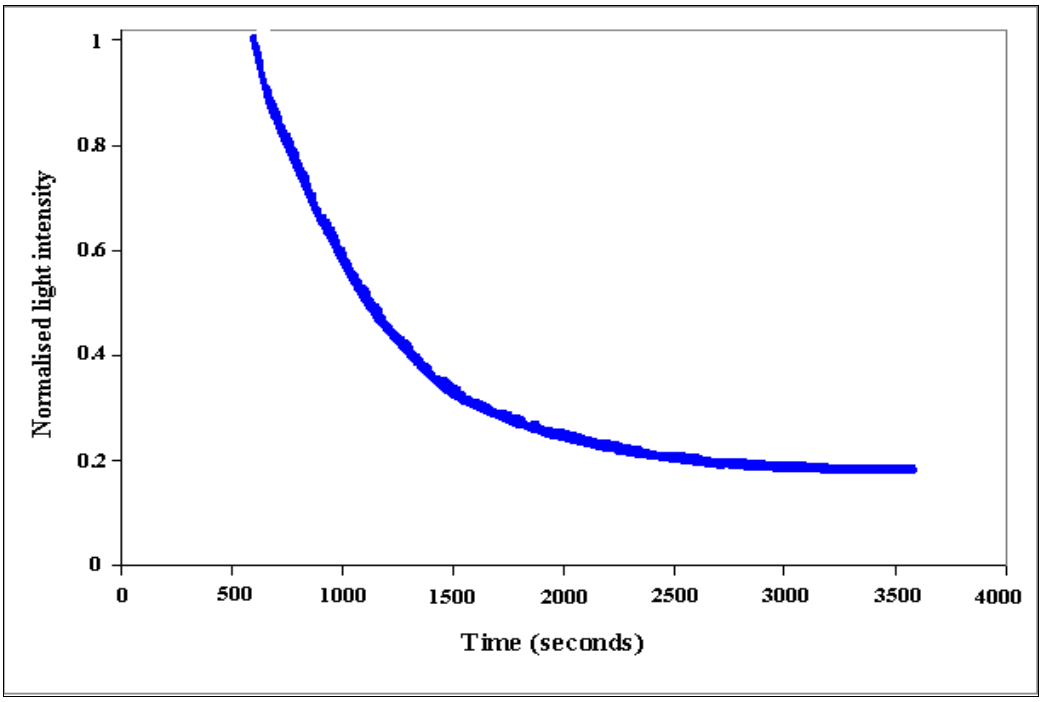

Figure 4.6(b): The dataset presented here is identical to that shown in Figure 4.6a but the transmitted light intensities to region A-K have been removed intentionally.

It can be concluded that the impregnation of the SDOF can be monitored by logging the transmitted light intensity through the fibre, as it is in touch with the resin.

4.5 Impregnation Monitoring of E-glass Fibre

A 28 cm length of water-sized E-glass fibre bundle was potted in a pair of SMA connectors with EPO-TEK® 310M and polished as described previously. The set-up was as described in Section 3.4 where the E-glass fibre bundle was illuminated with a laser light source (200 mW) at one end and a detector (an optical power meter) used for monitoring at the other. The resins was mechanically injected (using 2 injectors) on either side of the mould at a rate of 1.2 ml per hour.

The relationship between the transmitted light intensity and the impregnation time is shown in Figure 4.7(a). It is assumed here that the impregnation process started when EPO-TEK® 310M came in contact with the water-sized E-glass fibre. Although the resins was dispensed via an automatic pumping system (Aladdin programmable syringe pump by World Precision Instruments Inc., USA), it was impossible to dispense all of the required volume of resin into the mould in one attempt; it required a specified time to allow for proper impregnation of the fibre bundle within the depth of the mould after each period of dispensing. Consequently, resin delivery was interrupted manually every 6 cm (as judged visually).

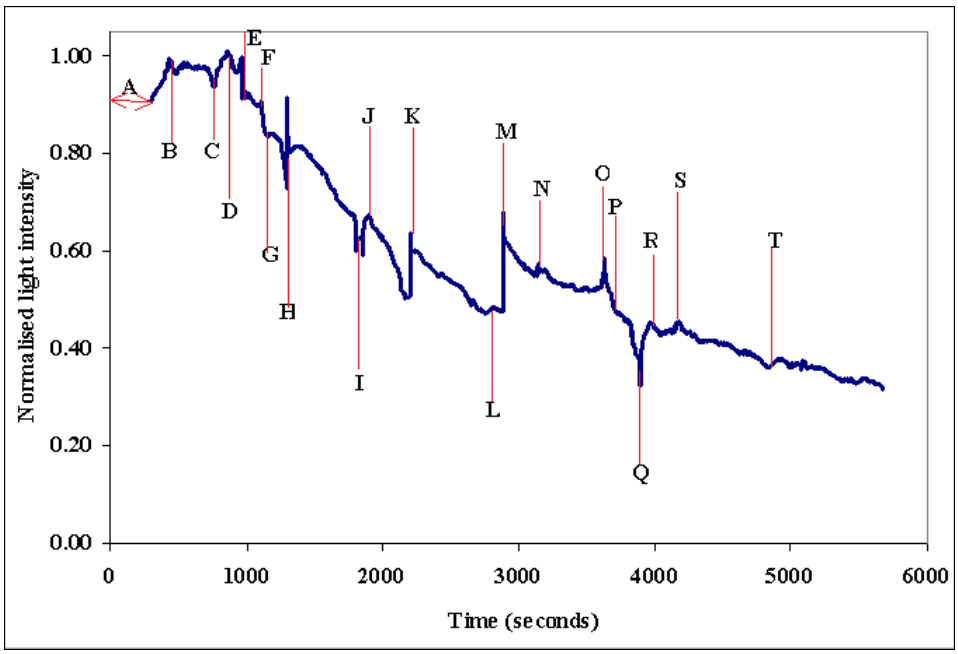

Figure 4.7(a): Graph showing changes in the light intensity during impregnation of water-sized E-glass fibres.

With reference to Figure 4.7(a), the portion labelled 'A' represent the moment the automated resin injection systems were switched on. However, the EPO-TEK® 310M (RI=1.4) had not reached the mould as it took some times before a smooth flow of the resin occurred. After the initial attenuation at point 'A', there seemed to be a fluctuation in the

transmitted light intensity at point ‘B’; this may be attributed to the resin dispensed from both syringes, spreading across the mould. The decrease in the normalised transmitting light intensity observed at points ‘C’ to ‘T’ as a function of time can be related to the impregnation length of the fibre bundle. Although the resin injection was better controlled by using the automated machine, as opposed to using the manual method adopted in the previous case, the dataset was still marred by the irregular fluctuation. The sharp fluctuations experienced at points ‘D’, ‘E’, ‘G’, ‘H’, ‘I’, ‘K’, ‘L’, ‘M’, ‘O’, ‘P’, and ‘Q’ may be due to:

(i) the manual pulsing of the two resin dispensing units;

(ii) the manner in which the resin wets and flows along the length of the fibre; and

(iii) entrapped air interfering with the impregnation process.

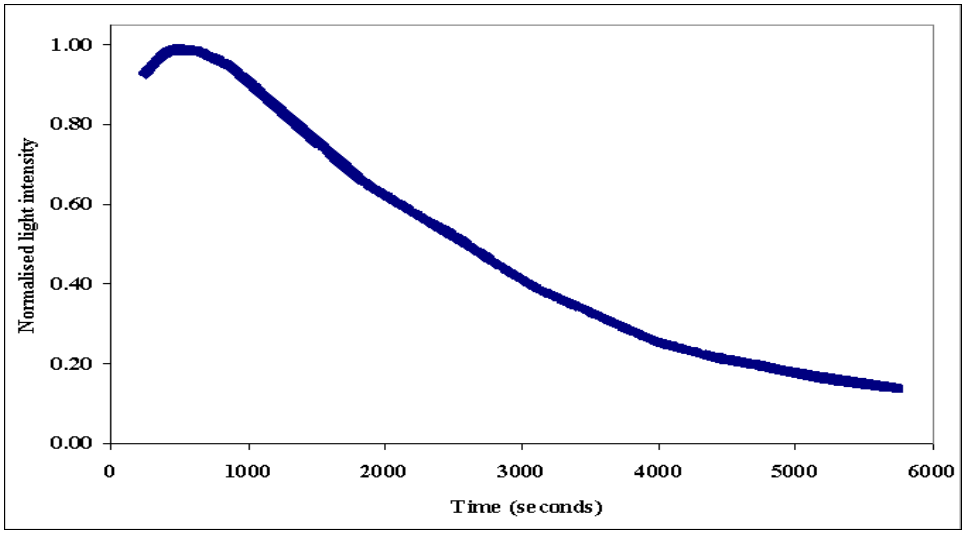

Figure 4.7(b): Graph showing the changes in the light intensity during impregnation of water-sized E-glass fibres as shown in figure 4.7a but having the spikes from points B to T removed.

As with SDOF, here the observed fluctuation in the data presented in Figure 4.7(a) were removed manually (intentionally) to demonstrate the attenuation of the transmitted light intensity as a function of the impregnation time.

With reference to Figure 4.7(b) (edited data), it can be concluded that the light transmission characteristics through E-glass can be used to monitor the impregnation process.

4.6 *In-situ* Monitoring of the Cross-linking Process

In Sections 4.1, 4.2 and 4.4, etching of the cladding on the SDOF, temperature sensing and *in-situ* monitoring of the impregnation/infiltration process were reported. This current section reports the *in-situ* monitoring of the cross-linking process using the same SDOF bundles.

The sensing principle used here is evanescent wave near-infrared (NIR) spectroscopy using the pre-heat-treated and etched SDOFs. The SDOF comprised of two bundles (3 g each) which were impregnated using EPO-TEK® 310M in a mould. The details of this were discussed in Section 4.4. The impregnated fibres and the mould assembly were transferred to an air-circulated oven that was set to 65 ^{0}C to enable cross-linking of the resin system.

Figure 4.8 shows typical spectra of the impregnated fibre bundle during cross-linking of the resin system. As reported by Xu, Fu and Schlup [50], the functional groups of interest in epoxy resin curing reactions typically have well-isolated absorption bands in the near-infrared (NIR) region of the spectrum between 1000 and 4000 cm^{-1}, as shown in Figure 4.8. The peak designated as ‘B’ represents the combination band of secondary and primary amine while the spectra peak denoted as ‘E’ represents the primary amine peak. The peak

denoted as ‘A’ is the hydroxyl group overtone whilst the peak ‘C’ represents the aromatic ring C-H stretch combination.

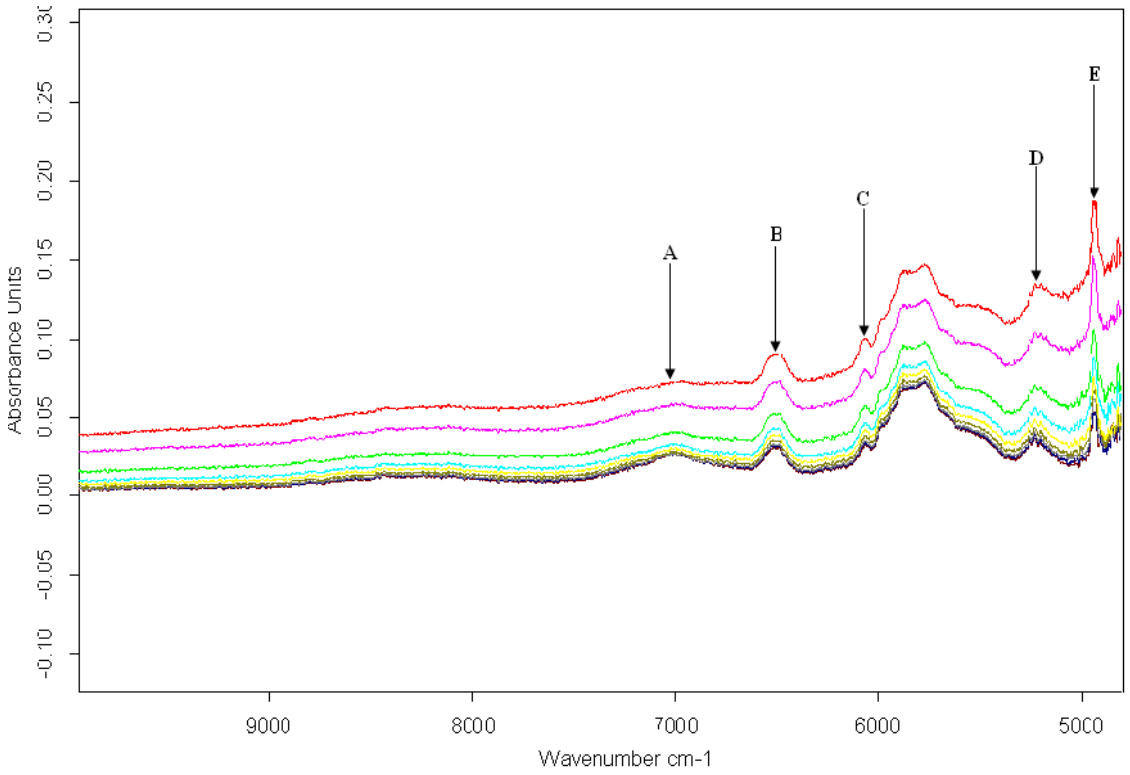

Figure 4.8: NIR absorption spectrum for the impregnated SDOF bundle during cross-linking process.

As shown in Figure 4.8, the hydroxyl group overtone peak denoted as ‘A’ and the aromatic ring C-H stretch combination peak ‘C’ were negligible and therefore not considered for further analysis in this work. Also, the spectrum pattern between 4000 and 5000 cm^{-1} where the epoxy peak was present were not clear as a result of the noisy nature of the spectra; this may be due to:

(i) the length of the SDOF sample used for this experiment (1 m);

(ii) surface contamination as this fibre bundle had been subjected to the temperature monitoring and impregnation experiments previously; and

(iii) contamination of the end-faces of the SMA connector.

Due to time constraints, it was not possible to manufacture new bundles for any repeat experiment.

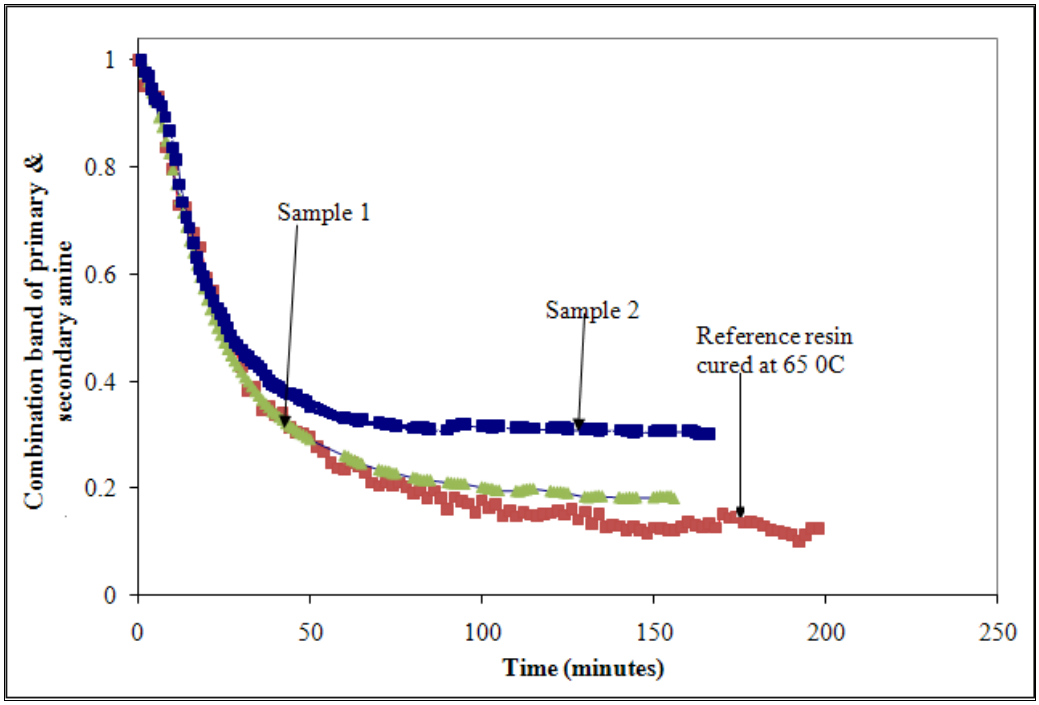

Figure 4.9: Graph showing comparison of absorption of combination band of primary and secondary amine in an *in-situ* curing kinetic of epoxy resin between samples 1 and 2 and conventional sample cured at the same temperature of 65 ^{0}C.

Further analysis of these peaks was carried out by calculating the peak area within combination band of secondary and primary amine. These datasets were compared with an established dataset (conventional NIR transmission spectroscopy) obtained from the curing of EPO-TEK® 310M and its associated hardener at the same temperature (65 ^{0}C) as used in this experiment.

Figure 4.9 shows the consumption of combination band of primary and secondary amine peak for the two samples used in this study. The behaviour is seen to be similar until

approximately 40 minutes of the cross-linking process when they were seen to deviate. However, by comparing the rate of depletion of the combination band of primary and secondary amine for sample 1 with that obtained via a conventional NIR transmission spectroscopy, a good correlation was obtained for up to 50 minutes which is approximately 75 % of the cross-linking reaction.

The observed deviation of the various datasets towards the end of the reactions may be attributed to the following issues in evanescent wave spectroscopy:

(i) the signal-to-noise reduces significantly towards the end of the cross-linking process [51]. This may be due to the fact that once the reagents at the surface of the fibres are depleted; the reactivity is likely to be lowered. Issues relating to surface contamination were mentioned in the literature earlier.

An attempt was made to further analyse the primary amine peak but the noise signal activity at this band made it impossible to come up with a meaningful result, and therefore, it was discarded.

Despite the inadequacies shown in the datasets, it can be concluded that evanescent wave near-infrared (NIR) spectroscopy can be used for monitoring the cross-linking process in composite manufacturing. Further research is required to establish the consistency of the evanescent wave spectra.

This section has demonstrated that the life cycle of a reinforced fibre composite can be monitored from the impregnation process to the curing or processing stage. Here, the reinforcing fibres act as sensor as previously mentioned. It is also worth noting that

previous researchers have demonstrated that surface treatment process can be monitored, for example, silane treatment [52].

Sections 4.2, 4.4, 4.5, and 4.6 have demonstrated that SDOF and E-glass fibre can be used for monitoring the defects in the fibres, the impregnation process and subsequent curing or cross-linking process of resin system. Meanwhile, the next section reports the development of image analysis routines which can be used to detect the fracture of individual filament in the bundle.

4.7 Image Analysis

The image analysis routines developed by Malik *et al.* [1] for analysing the fracture behaviour of SDOFs when used as a light guide were employed in this section. The specimens were prepared and end-tabbed as described in Section 3.3. Figure 4.10(a) shows the illuminated ends of the SDOFs, in the unloaded state, using the high-speed camera. The plot in Figure 4.10(b) illustrates the initial images after adjusting the background and luminance threshold using image analysis routines within Matlab 8.0. Further processing of this image was carried out to assign the x- and –y coordinates for each of the individual fibre as shown in Figure 4.10(c). The processing of these images and the quality of the output shown in Figure 4.10(c) was found to be adequate for the studying of the fracture of reinforcing SDOF. It was also determined that Matlab routines were able to identify the centroidal position of each fibre, using x - y coordinates and also to identify each fibre to an accuracy of approximately 94 ± 2 %.

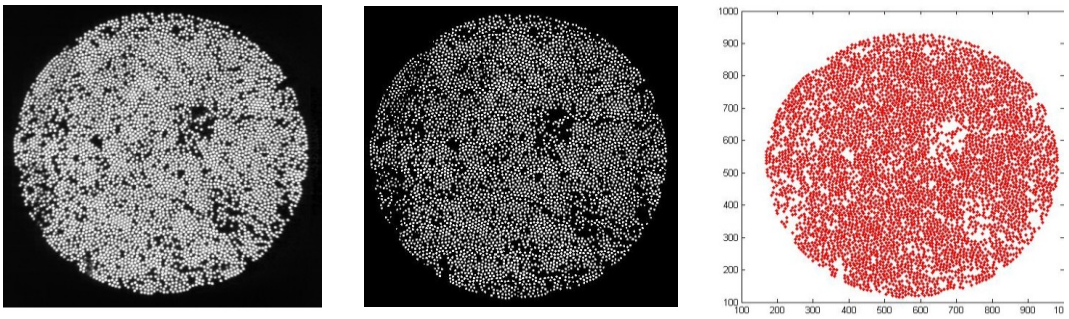

(a) First image (b) Background-corrected (c) X-y coordinates

Figure 4.10(a-c): Image analysis captured by the high-speed camera and subsequently processed with Matlab 8.0 software [1].

As mentioned above, the macro that was developed by Malik *et al* [1] in Matlab 8.0 was used to read the first image as it can identify an individual fibre as an entity. By using these same techniques for the whole images, light intensities for each fibre were calculated at their coordinate positions. Figure 4.11(a to d) shows the light intensity plots generated from Matlab for each image shown. Image 'a' is the 600th frame while 'b', 'c' and 'd' are 1,800th , 2,400th and 4,800th frames captured, respectively by the high-speed camera at various stages of the testing of SDOF bundle. The light intensity calculation for each of them are shown in 3D format in Figure 4.11(e to h) which show the location of the individual fibre using x- and y- coordinates for each light intensity. The measured light intensity was then averaged for each image and then plotted against time.

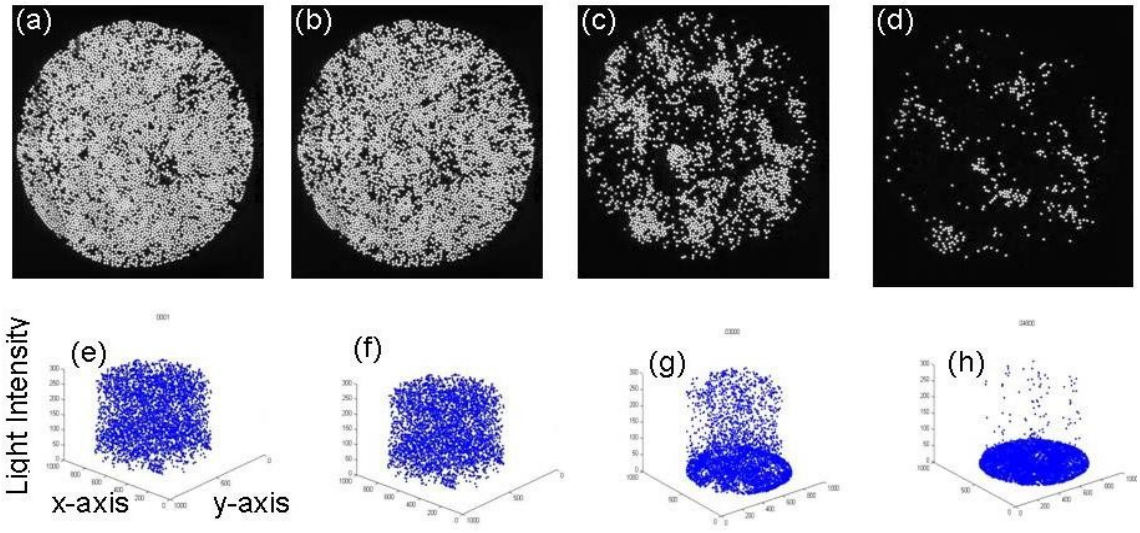

Figure 4.11: (a-d) Show series of images generated by using Matlab, and these are in relation to 600th, 1,800th, 2,400th, and 4,800th frames captured by the high-speed camera at various stages of tensile testing of small diameter optical fibre bundle. The transmitted light intensity analysis carried out on these images produced Figures 4.11(e-h), where x and y axes indicate the position of an individual fibre while z-axis represents the position of the light intensity of each fibre [1].

4.7.1 Tensile testing of fibre bundle

The image analysis routine developed using Matlab can identify either surviving or fractured fibres during mechanical loading of a specimen. This routine was used to investigate and monitor fibre behaviour prior to fracture. Figure 4.12(a-c), shows three sequential frames taken during tensile loading of SDOF bundle. The arrow in each frame indicates the position of a fibre before, during, and after fracture respectively. It is shown in Figure 4.12(a-c) that light attenuation occurs just prior to failure and the same trend was applicable to all of the fibres in the bundle, thus enabling the fracture sequence of the fibres to be monitored. At the time of writing the author was not aware of any previous publications where this technique was reported.

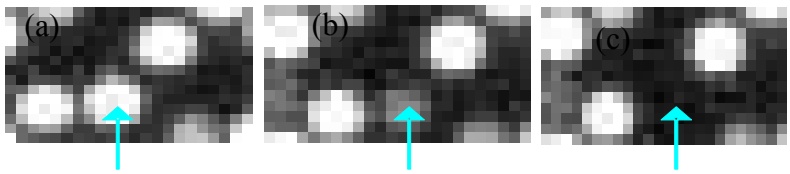

(a) whilst being loaded in tension; (b) just prior to fracture; (c) immediately after fibre fracture.

Figures 4.12 (a-c): Identification of an individual fibre fracture by monitoring the transmitted light intensity [1].

Figure 4.13 (a, b, and c) shows the transmitted light intensity through the as-received SDOF, heat-treated SDOF, and E-glass fibre bundle as a function of applied load. In the majority of bundle tested, a rapid decrease in the transmitted light intensity was noticed at or after 90 % of the applied load. A similar trend was observed with the other similar fibre bundles as shown in Figure 4.14. These datasets demonstrate that the fibre bundle did not experience a catastrophic failure due to the load imposed which suggests that the reduction may be due to:

(i) the variability of tension between various filaments in the bundle;

(ii) the transfer of the loads from the weaker fibre filaments to the surviving ones due to their sequential failure; and

(iii) the strength distribution of the fibre.

With reference to Figure 4.13(a), there is a small but noticeable decrease in the transmitted light intensity which may have occurred as a result of fibre bundle being loaded in tension. This may be due to the fracture of some of the fibres in the end-tab region and fraction of the weakest fibres. The peak failure load of the as-received SDOF bundle was 525 N. A clear downturn in the transmitted light intensity is observed after load of approximate 470

N was reached. A significant faster rate of attenuation is noticed as the applied load increases.

As seen in Figures 4.13 and 4.14, the transmitted light intensity for the bundles did not experience an abrupt attenuation behaviour just after the peak load. This suggest that some of the fibre filaments still continue to transmit light after the peak load was reached. This is possible since the strength of the filaments in the bundle is not equal; so there is tendency that the stronger fibres carry the load as the weaker fibres fracture. This is in contrast to the event in a composite where the fracture of a fibre does not result in a total loss of load bearing capacity; whereas in the case of the fibre bundle, once a fibre fractures, it transfers the load to the surviving fibres.

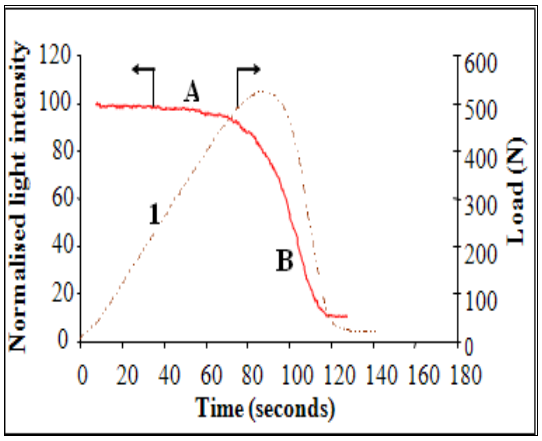

(a) As-received SDOF bundle.

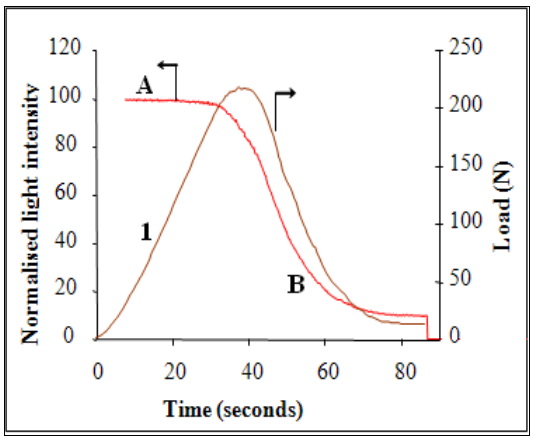

(b) Heat-treated SDOF bundle.

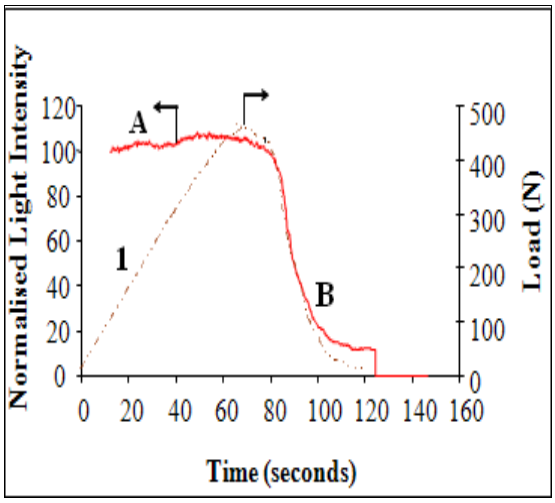

(c) Water-sized E-glass fibre bundle.

Figure 4.13 (a, b and c): Graphs showing normalised transmitted light intensity load versus time for the (a) as-received SDOF, (b) heat-treated SDOF and (c) water-sized E-glass fibre bundles (Sample 1).

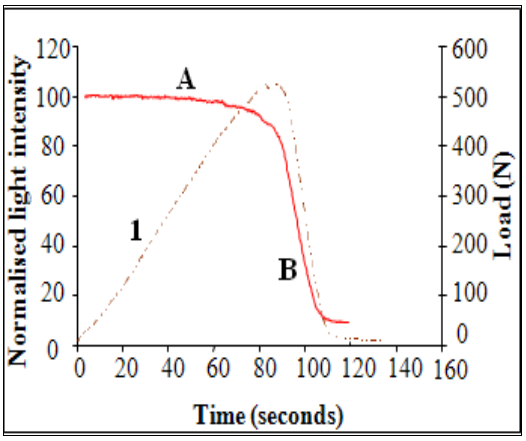

(a) As-received SDOF) bundle.

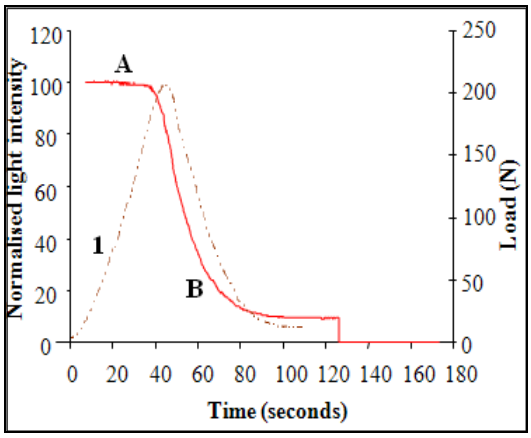

(b) Heat-treated SDOF bundle.

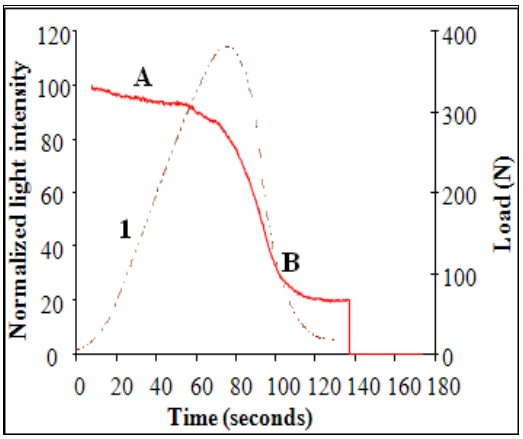

(c) Water-sized E-glass fibre bundle.

Figure 4.14 (a, b and c): Graphs showing normalised transmitted light intensity load versus time for the (a) as-received SDOF, (b) heat-treated SDOF and (c) water-sized E-glass fibre bundles (Sample 2).

Figure 4.13(c) shows the normalised light intensity and applied load as a function of time for the water-sized E-glass fibre bundle. Here, a small increase in the transmitted light intensity is noticed. This may be due to the following reasons:

(i) the inherent twist in the fibre which eventually straighten out due to increase in applied load; and

(ii) the uneven tension in the fibre bundle.

Unlike the as-received SDOF bundle where a continuous decrease in the attenuation of the transmitted light intensity was noticed before the peak was reached, here, the E-glass fibre bundle maintains its transmitted light intensity until peak load was nearly reached. After the peak load was reached, a rapid attenuation in the light intensity was observed.

Table 4.1: Comparison of normalised transmitted light intensity slopes between two different bundles of as-received SDOF, heat-treated SDOF and water-sized E-glass fibres.

Figure / Sample number	Fibre bundle type	Slope at '1' (Load/Time)	Slope at 'A' (Light intensity/Time)	Slope at 'B' (Light intensity/Time)
Figure 4.13 (Sample 1)	As-received SDOF	7.0	0.1	3.0
	Heat-treated SDOF	6.9	0.15	4.0
	Water-sized E-glass	7.5	(0.2)	5.5
Figure 4.14 (Sample 2)	As-received SDOF	7.1	0.2	2.1
	Heat-treated SDOF	6.5	0.1	3.0
	Water-sized E-glass	7.4	0.2	2.3

By comparing Figure 4.13 (a and b) for the as-received SDOF and 'heat-treated' SDOF respectively, the following comments can be made:

(i) the peak failure load sustained by the heat-treated fibre bundle was half of that obtained for the as-received. This may be due to the embrittlement of the fibres after the binder was removed via pyrolysis and the subsequent processing that the bundles were subjected to; and

(ii) the onset of fibre fracture was significantly earlier for the heat-treated fibres. This may be attributed to the fragility of the fibres due to pyrolysing the coating on the bundle. Due to time constraint, no attempt was made to study this further.

Six individual test specimens were tensile tested for the three types of fibre bundles used in this study. Figure 4.14 (a, b, and c) show attenuation and load versus time traces for the different test specimen (Sample 2).

With reference to Figure 4.13 and 4.14(a, b, and c), it is important to know that it is virtually impossible to produce identical fibre bundles. This is because:

(i) the number of un-fractured fibres in any given bundle will be different;

(ii) the degree of tension in the fibres will not be the same;

(iii) the relative tension in the fibre bundle will be variable, although due care was taken to try and maintain a constant tension;

(iv) a significant variation in the fibre was observed; and

(v) it was always not possible to ensure that the end-tabbed fibre bundles were loaded in the tensile tests machine without undue variable tension being introduced in the fibres during the clamping process.

With reference to the data presented in Figure 4.14, the general trends in the datasets for the three classes of material tested are similar to that described previously. The following section discusses some of the obvious differences that were observed with each class of material.

Table 4.1 presents a summary of the slopes of the datasets in Figures 4.13 (a – c) and 4.14 (a – c). In Table 4.1, 'slopes' 1, A, and B correspond to:

(i) "1" = the initial loading rate of the fibre bundle;

(ii) "A" = the rate of attenuation during the initial mechanical loading phase of the bundle; and

(iii) "B" = the rate of attenuation of the light during the failure of the bundle after the peak load.

This analysis was carried out only for the graph presented in Figures 4.13 and 4.14. The rates of loading for the different types of fibre bundles were similar. This is reasonable as the number of glass fibre filaments were approximately similar. The following conclusion can be made for 'slope A' in Table 4.1:

(i) the rate of attenuation of the transmitted light in the initial loading period (up to approximately 60 % of the peak load was lowest for the SDOF;

(ii) the variability in the datasets for the heat-treated SDOF is apparent in Table 4.1. The heat-treatment of the SDOF at 450 ^{0}C for 6 hours was found to embrittled them. The actual reasons for this were not envisaged but the following issues may have contributed to the weakening of the fibres: the heat-treatment resulted in the oxidation of the organic materials (processing aids, lubricant, only static, etc). Therefore, the fibres are no longer 'protected' by the coating and have their serviceability to surface abrasion increased. It is also known that the mechanical properties of glass fibres can be affected adversely by adsorption moisture [53];

(iii) when the coating was heat-treated, the cohesion of the fibre bundle was lost and the individual filament was relating free to 'flex'. Therefore, it is reasonable to assume that probability of damage to the individual filament in a bundle that has been heat-treated would be higher;

(iv) with regard to the loss of cohesion of the fibre bundle after heat-treatment, the retention of relatively uniform tension in the filament may not be possible. Therefore, not all the filaments in the bundle would be loaded uniformly;

(v) it is not known if the heat-treatment resulted in migration of additives or dopants from the SDOF [54]; and

(vi) with regard to the water-sized E-glass fibres, the increase in the light intensity as a function of applied load (see Figure 13c) may have been due to the filaments straightening out during tensile loading.

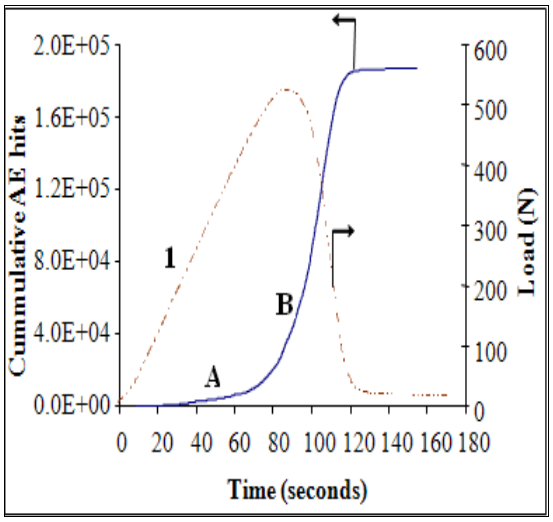

a) As-received SDOF bundle.

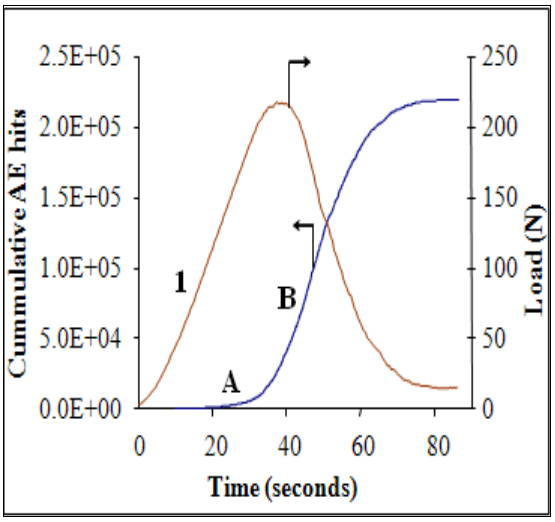

(b) Heat-treated SDOF bundle.

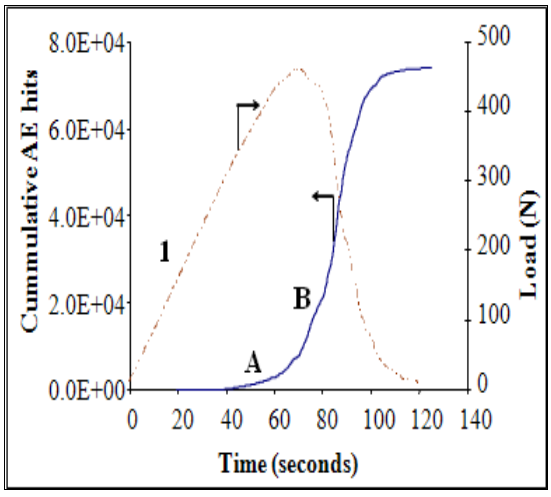

(c) Water-sized E-glass fibre bundle.

Figure 4.15 (a, b and c): Graphs showing cumulative AE hits and load versus time for the (a) as-received SDOF, (b) heat-treated SDOF and (c) water-sized fibre bundles (Sample 1).

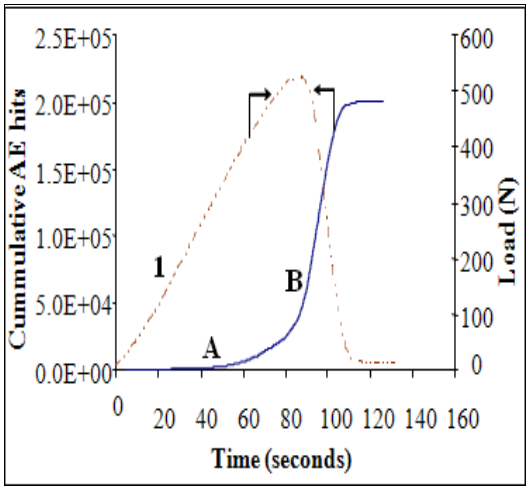

(a) As-received SDOF bundle.

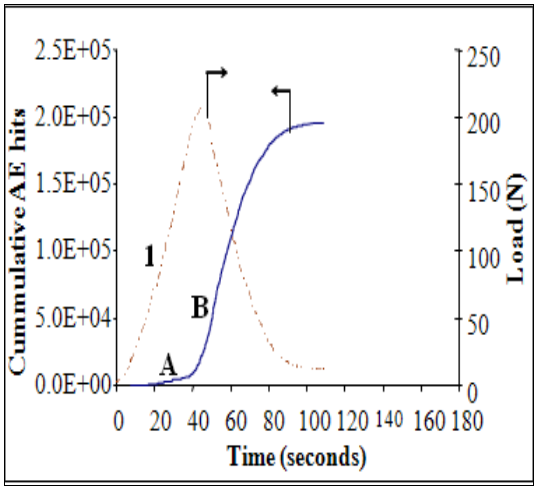

(b) Heat-treated SDOF bundle.

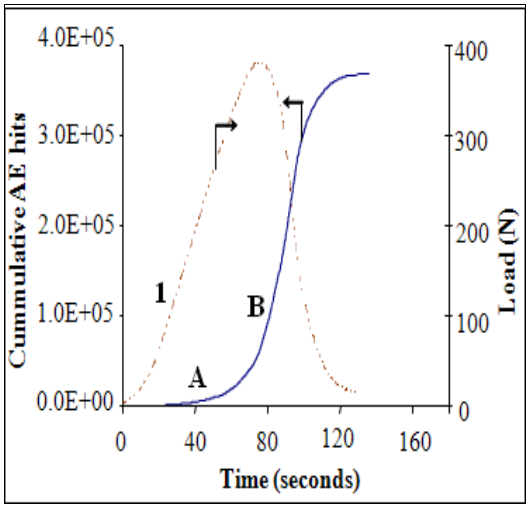

(c) Water-sized E-glass fibre bundle.

Figure 4.16 (a, b and c): Graphs showing cumulative AE hits and load versus time for the (a) as-received SDOF, (b) heat-treated SDOF and (c) water-sized E-glass fibre bundles (Sample 2).

Figure 4.15 (a-c) shows the cumulative AE hits and load as a function of time for the (a) as-received SDOF bundles, (b) heat-treated SDOF bundle and (c) the water-sized E-glass fibre

bundles. Six bundles of each type were tensile tested and two representative sets of graphs are discussed here.

With reference to Figure 4.15 (a-c), a common characteristic feature is that the AE hits continue well after the peak load was reached. This is also the case with the data presented in Figure 4.16 (a-c).

As with the light intensity and load versus time data presented previously, the slopes at specified region in the load versus time and cumulative AE hits versus time were calculated. The codes shown in Figures 4.15 (a-c) and 4.16 (a-c) are as follows:

(i) slope "1" represents the linear position of the load/time trace;

(ii) slope "A" represents the initial rate of cumulative AE hits; and

(iii) slope "B" represents the region correspond to the rapid increase in the rate of cumulative AE hits.

The calculated slopes are summarised in Table 4.2

Figure / Sample No.	Fibre bundle	Slope '1' (Load/ Time)	Slope 'A' (Cumm. AE/Time)	Slope 'B' (Cumm. AE/Time)	Max. number of AE	Peak load
Figure 4.15 (Sample 1)	As-received SDOF	7.0	217	4513	1.9E+05	525
	Heat-treated SDOF	6.9	595	4554	2.2E+05	220
	Water-sized E-glass	7.5	540	16670	7.5E+04	460
Figure 4.16 (Sample 2)	As-received SDOF	7.1	416	5508	2.0E+05	525
	Heat-treated SDOF	6.5	667	8272	2.0E+05	207
	Water-sized E-glass	7.4	625	10500	3.8E+05	380

Table 4.2: Comparison of the slopes, maximum number of AE, and peak load between two different samples of as-received SDOF, heat-treated SDOF, and water-sized E-glass fibre bundles.

With reference to Table 4.2, the rates of loading (slope 1) for the three classes of fibre bundles were similar.

The cumulative AE hits versus time plot shows the evolution of damage in a test specimen. Hence, the cumulative number of AE hits was calculated by successive edition of AE hits as recorded from each AE signal detected as the test progressed. In Table 4.2, the slope "A" for the as-received SDOF in sample 1 is 217 AE hits/seconds at approximately 60 seconds. At this point the failure load experienced by the sample was 460 N (85 – 90 % of the peak load). The slope of cumulative AE hits (slope "B") increased significantly by approximately 20 times of its initial value i.e. 4513 AE hits/seconds. As mentioned previously, the change in slope of AE plot is indicative of damage occurring in the test specimens [55], [56]. After the peak load (525 N) was reached; the plot of AE hits kept increasing. This was indicative of the AE activities occurring in that sample.

A similar trend was observed in the case of heat-treated SDOF. However, initial slope at slope "A" shows a 2½ times greater than that of as-received SDOF. The most likely cause of this change was the effects of heat-treatment and binder removal by pyrolysis as discussed in Sections 3.2.2 and 4.1. It was noticed by visual inspection that heat-treatment induces brittleness; therefore, more AE hits were recorded in the initial phase (slope "A"). The slope "B" for both as-received and heat-treated samples was similar.

In the case of water-sized E-glass fibre bundle, slope "A" is greater than that of the as-received SDOF. This may be due to the fact that water-sized E-glass fibres were un-sized and therefore, may experience comparatively more inter-fibre friction [55]. Therefore, more AE hits were produced during tensile testing of E-glass fibre when compared with the as-received SDOF. At approximately 50 seconds, the load on the sample was 400 N (85 % of peak load). At this point, the slope "B" of the cumulative AE hits increased ~30 times. This

was due to the damage occurring in the fibre bundle when the peak load was about to be reached.

In conclusion, the changes in AE plots were predominantly dependent on: the load/time trace of the sample; the failure modes in the bundle; and the interaction of individual fibres in the bundle. The detailed analysis of AE data is outside the scope of this thesis. However, the amplitude and frequencies of AE signal give detail characteristics of failure load in the fibre bundles [1], [55], [57].

4.7.2 Tensile testing of composites

Examples of typical responses of the composites to tensile loading and the resultant change in transmitted light intensity of the reinforced as-received SDOF, heat-treated SDOF and E-glass fibre composites are shown in Figure 4.17 (a, b and c). The data for another set of samples are shown in Figure 4.18 (a, b and c). Also, the cumulative AE hits and applied load as a function of time for these composites are shown in Figure 4.20 (a, b and c) and Figure 4.21 (a, b, and c). The slopes on the light intensity were calculated and presented in Table 4.3 with the following notations:

(i) slope “1” represents the linear position of the load/time trace; and

(ii) slopes “A” and ”B” represent light intensity/time trace.

The results of the tests carried out on a number of specimens showed that the initial slopes for all the tested samples were similar. By considering the as-received SDOF composites, the normalised light intensity appeared steady until reaching the fracture point before experiencing an abrupt attenuation. This may be attributed to the fact that the transmitted light was not affected by the matrix (i.e. the fibres have a cladding) when compared with

the E-glass composite. All the test specimens of as-received SDOF composites fractured catastrophically at slope “B”. This is because the as-received SDOF compatibility with the matrix was very poor due to the cladding, which weakens the fibre/matrix interface. Also, according to Tsutsui *et al.* [58], the outer coating (cladding) of the as-received SDOF appeared to degrade the strength of the fibres less than the use of the uncoated fibres.

However, in the case of heat-treated SDOF, it was possible that 5 – 10 % of fibres fractured before peak load due to a comparatively better interface. This indicates that there was a better interaction between the heat-treated SDOF and the matrix than the as-received SDOF discussed in the previous paragraph. Therefore, the change in the light intensity at slope “B” was mainly due to fracturing fibres before the peak load.

In the case of water-sized E-glass fibre composites, the slope of light intensity at “A” was decreasing at approximately 40 % of ultimate tensile strength (UTS) than the as-received SDOF and heat-treated SDOF composites. As mentioned previously, the strength failure of matrix was lower than for the E-glass fibre (matrix failed earlier than fibre). Therefore, in the case of E-glass fibre composite the failure of matrix causes attenuation of light (the matrix was acting as cladding). Hence, there was possibility of change in optical properties of matrix under applied stress. Therefore, the net decrease in light transmission of water-sized E-glass composite before the peak load was due to fracturing fibres and matrix.

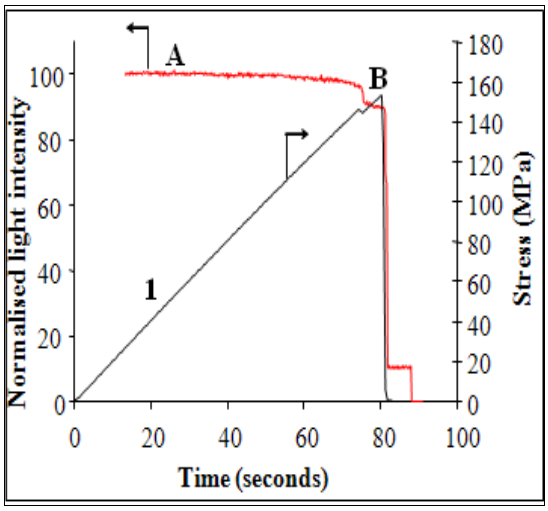

(a) As-received SDOF reinforced composite.

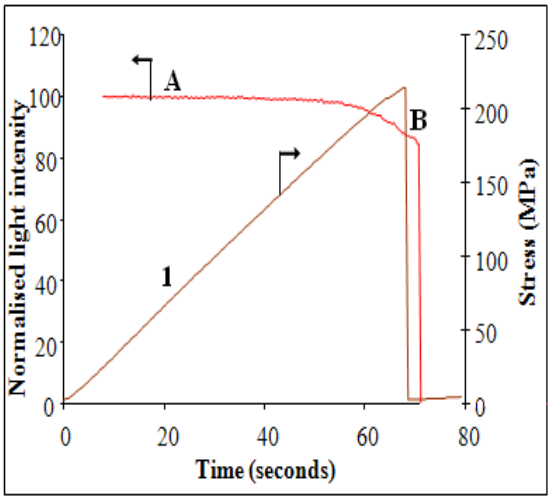

(b) Heat-treated SDOF reinforced composite.

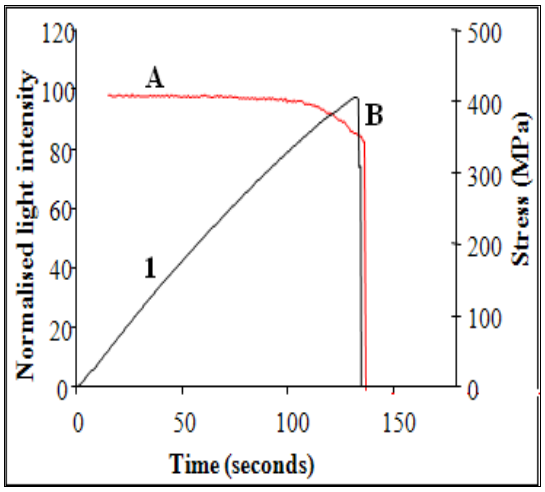

(c) Water size E-glass fibres reinforced composite.

Figures 4.17 (a, b and c): Graphs showing normalised transmitted light intensity and applied load versus time for the (a) as-received SDOF, (b) heat-treated SDOF, and (c) water-sized E-glass fibre reinforced composites respectively (Sample 1).

Generally, failure strain (~ 1 %) of matrix was lower than for the fibre [55]. This means that the matrix failed earlier and followed by matrix cracking.

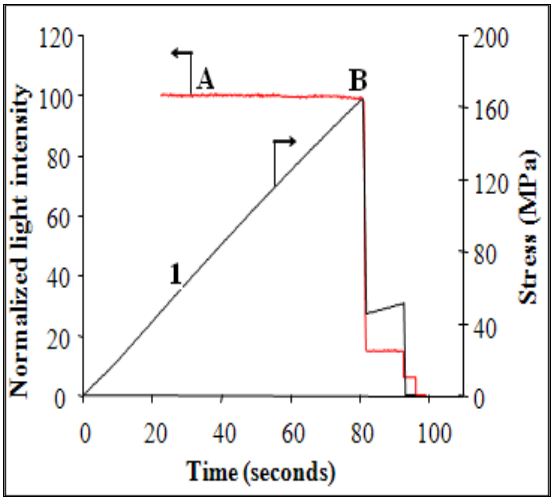

(a) As-received SDOF reinforced composite.

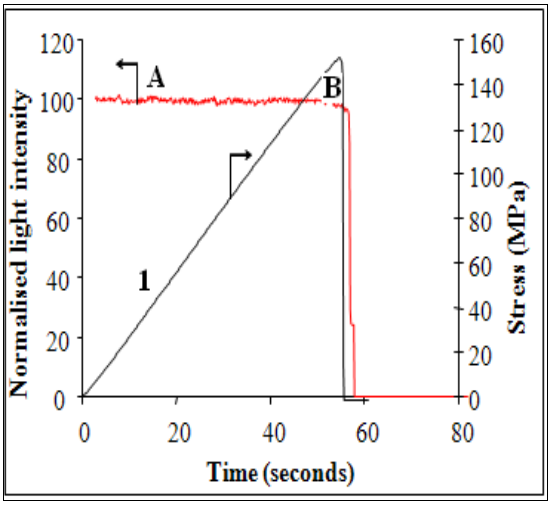

(b) Heat-treated SDOF reinforced composite.

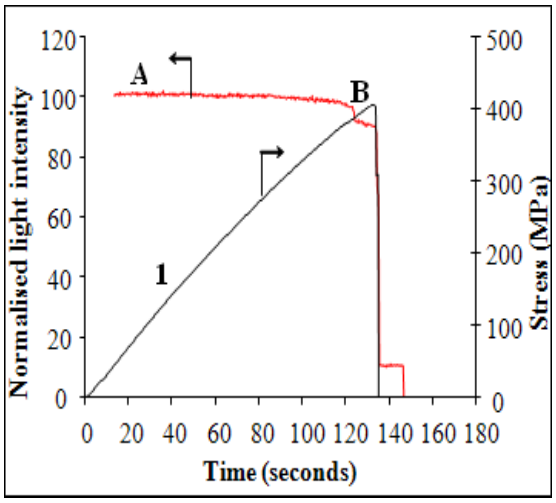

(c) Water-sized E-glass fibre reinforced composite.

Figures 4.18 (a, b and c): Graphs showing normalised transmitted light intensity and applied load versus time for the (a) as-received SDOF, (b) heat-treated SDOF and (c) water-sized E-glass fibre composites respectively (Sample 2).

In conclusion, it was demonstrated that the damage in the self-sensing composite specimens could be related to the change in light transmission of the reinforcing fibres.

Table 4.3: Comparison of slopes of normalised light intensity graphs of six samples of fibre reinforced composites manufactured from as-received SDOF, heat-treated SDOF, and water-sized E-glass fibre respectively.

Sample No.	Fibre used in the composite	Slope 1 (Stress/Time)	Slope A (Light intensity/Time)	Slope B (Light intensity/Time)
Sample 1	As-received SDOF	2.0	0.1	0.1
	Heat-treated SDOF	3.0	0.1	0.1
	Water-sized E-glass	3.7	0.1	-
Sample 2	As-received SDOF	2.0	-	-
	Heat-treated SDOF	2.8	-	0.1
	Water-sized E-glass	3.8	-	-
Sample 3	As-received SDOF	2.0	-	0.6
	Heat-treated SDOF	2.9	-	0.7
	Water-sized E-glass	3.0	0.1	0.1
Sample 4	As-received SDOF	2.3	-	-
	Heat-treated SDOF	3.7	-	-
	Water-sized E-glass	3.4	0.1	-
Sample 5	As-received SDOF	2.4	-	-
	Heat-treated SDOF	2.5	-	0.1
	Water-sized E-glass	3.5	0.1	-
Sample 6	As-received SDOF	2.0	-	-
	Heat-treated SDOF	3.0	0.1	0.1
	Water-sized E-glass	3.7	0.1	-

- indicate slopes that were not calculated due to the horizontal nature of normalised intensity/time trace at these points.

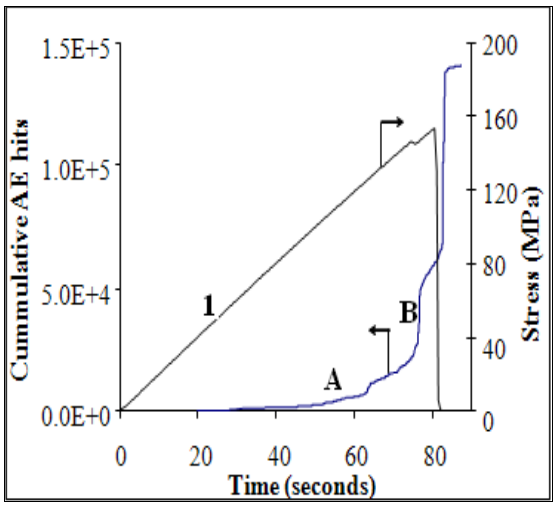

(a) As-received SDOF reinforced composite.

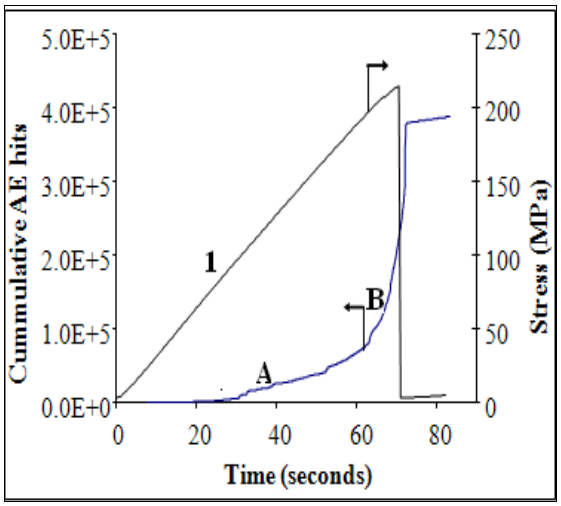

(b) Heat-treated SDOF reinforced composite.

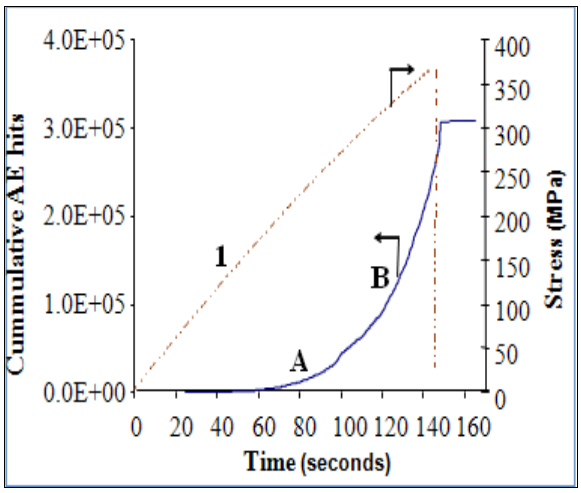

(c) Water-sized E-glass fibre reinforced composite.

Figures 4.19 (a, b and c): Graphs showing cumulative AE hits and applied stress versus time for the (a) as-received SDOF, (b) heat-treated SDOF and (c) water-sized E-glass fibre composites respectively (Sample 1).

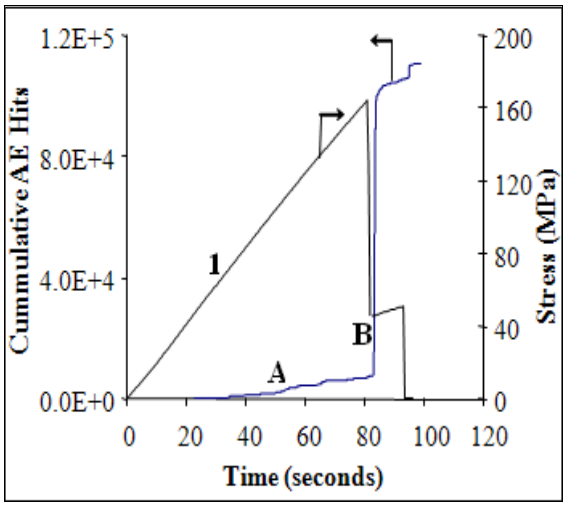

(a) As-received SDOF reinforced composite.

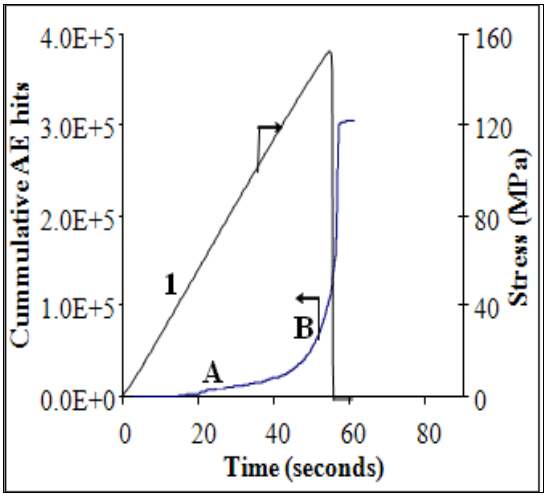

(b) Heat-treated SDOF reinforced composite.

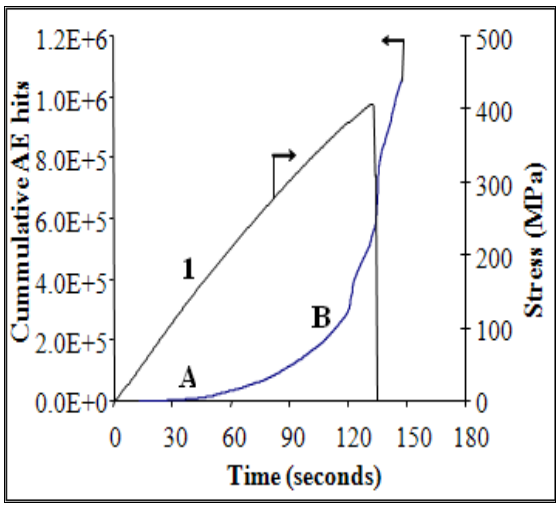

(c) Water-sized E- glass reinforced composite.

Figure 4.20 (a, b and c): Graphs showing cumulative AE hits and applied stress versus time for the (a) as-received SDOF, (b) heat-treated SDOF, and (c) water-sized E-glass fibre composites respectively (Sample 2).

Table 4.4: Comparison of slopes of cumulative AE hits of six samples of fibre reinforced composites manufactured from as-received SDOF, heat-treated SDOF, and water-sized E-glass fibre respectively.

Sample No.	Reinforcement used in the composite	Slope 1 (Stress/Time)	Slope A (Cumm. AE/Time)	Slope B (Cumm. AE/Time)	Max. AE hits	Peak stress (N)
Sample 1	As-received SDOF	2.0	250	1500	2E+05	155
	Heat-treated SDOF	3.0	1250	12315	4E+5	215
	Water-sized E-glass	3.7	1333	17511	1E+06	400
Sample 2	As-received SDOF	2.0	178	-	1E+5	168
	Heat-treated SDOF	2.8	638	13475	3E+5	153
	Water-sized E-glass	3.8	1667	16571	1E+6	410
Sample 3	As-received SDOF	2.0	200	3250	1E+05	160
	Heat-treated SDOF	2.6	769	11715	5E+05	175
	Water-sized E-glass	3.0	1428	16667	7E+5	350
Sample 4	As-received SDOF	2.3	228	1600	1E+05	150
	Heat-treated SDOF	3.2	900	14025	3E+05	155
	Water-sized E-glass	3.7	1333	17441	6E+05	390
Sample 5	As-received SDOF	2.4	280	-	2E+05	180
	Heat-treated SDOF	2.8	865	13120	3E+05	172
	Water-sized E-glass	3.5	1213	17136	4E+5	380
Sample 6	As-received SDOF	2.0	186	3210	1E+05	155
	Heat-treated SDOF	3.0	725	12314	4E+05	180
	Water-sized E-glass	3.7	1585	15245	1E+6	400

- indicate slopes that were not calculated due to the step-wise nature of the AE/time trace.

Figure 4.19 (a-c) shows the plot of cumulative AE hits and stress as a function of time for the (a) as-received SDOF composite, (b) heat-treated SDOF composite and (c) water-sized E-glass fibre composite. Six sets of these composites were tested and two representatives are presented here (Figures 4.19 (a-c) and 4.20 (a-c)) while slopes for each one of the samples are presented in Table 4.4, with the same notations defined earlier in this Section.

In Figure 4.19 (a) (as-received SDOF composite) slope at "A" shows a gradual increase in cumulative AE hits curve before a sudden change of slope just before fracturing. The presence of binder made the fibre and matrix to behave independently, the aftermath of which might have caused an irregular transitional cumulative AE hits/seconds curve pattern as occurred in slope "B" in sample 1 or where the slope experienced catastrophic change at peak load (see Figures 4.19 (a) and 4.20 (a)).

At approximately 70 seconds of the testing time, there was a rapid change in the rate of cumulative AE hits. Here, the stress experienced by this sample (see Figure 4.19 (a)) was approximately 140 MPa which is about 85 % of the peak stress. By comparing this with the heat-treated SDOF composite shown in Figure 4.19 (b), the cumulative AE hits/second curve formed a smoother transition as there was a gradual increase of cumulative AE hits from slope "A" to "B" similar to E-glass composite. This may be due to better compatibility of properties between fibre and matrix which might be due to binder removal through pyrolysis discussed in Section 3.2.2 and 4.2. When the testing time was 50 seconds, the stress imposed on sample 2 was approximately 150 MPa which is about 70 % of the peak stress.

Gradual increase in AE hits at slope "B" might have been caused by:

(i) matrix cracking;

(ii) fibre/matrix failure;

(iii) interface failure;

(iv) debonding of fibre from the matrix; and

(v) fibre fracture.

The detail analysis of AE data (amplitude, peak frequency and average frequency) give information on damage pattern occurring in the composite during tensile testing.

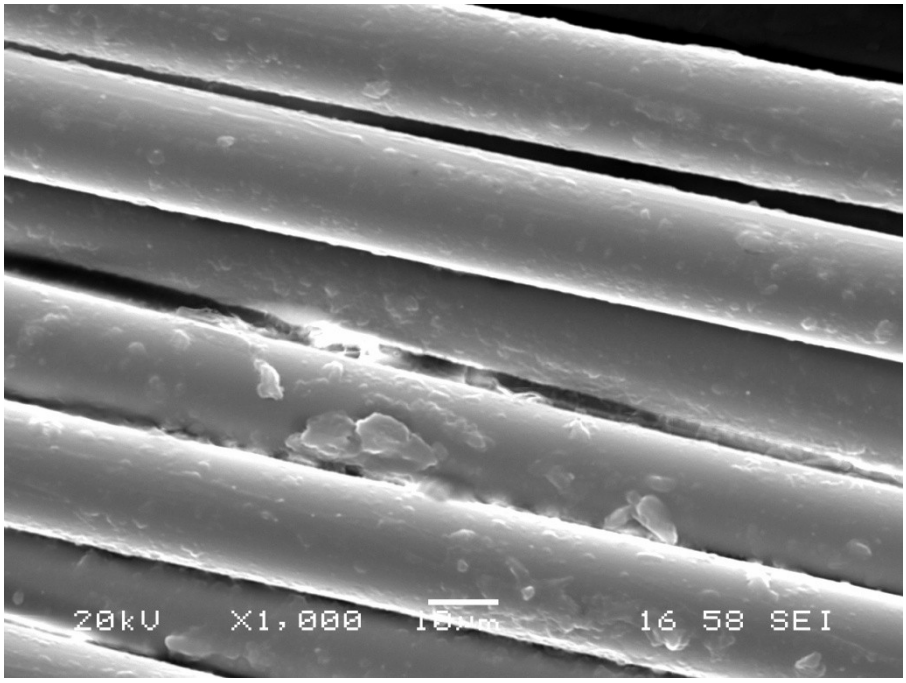

Figure 4.21: SEM image of as-received SDOF.

On comparing Figure 4.19(a) and Figure 4.20(a) (as-received SDOF composite), a stepwise increase in the cumulative AE-hits is observed. This may be due to poor bonding and the formation of longitudinal splits in the test specimen during tensile loading. In Table 4.4, it is seen that the slopes for the load/time traces are slightly higher for the heat-treated fibre when compared to the as-received SDOFs. This was probably due to the presence of a

higher binder content in the as-received SDOF. Evidence for this is shown in Figure 4.21. Figure 4.22 shows that the surface of the SDOF that were heat-treated at 450 ^{0}C for 6 hours were relatively free of the binder.

In Figure 4.19(c) and Figure 4.20(c), (water-sized E-glass fibre composite), the slopes for the load/time traces were similar for the two examples. This is reasonable as the manufacturing techniques were to produce the composition and the fibre volume fractions that were similar.

In Figures 4.19(c) and Figure 4.20(c), expected increase in the AE counts were observed prior to failure.

In Table 4.4, the maximum numbers of cumulative AE hits for the heat-treated SDOF were higher when compared to the as-received SDOF fibres. This is because the heat-treatment oxidised the organic binder and exposed the surface of the fibres to damage from observation. It is also possible that high binder content attenuated the AE signal. The number of cumulative AE hits for the water-sized components was similar. The reasons for this were observed, previously.

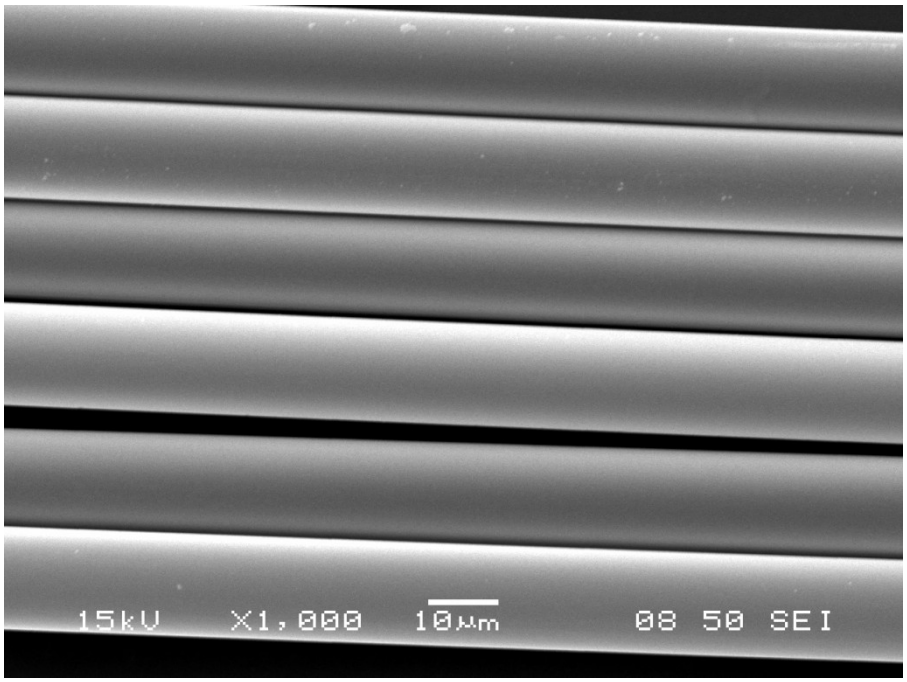

Figure 4.22: SEM image of heat-treated SDOF.

In Table 4.4, the failure stresses for the as-received SDOF composites were smaller. However, this was not the case with the heat-treated SDOF. In this study, a minimum of 6 samples were manufactured and tested; the results are summarised in Table 4.4. It is apparent that the heat-treated samples exhibits more scatter.

Chapter 5

5.0 Conclusion

Conventional E-glass fibres were used as light guides. This was achieved by selecting a thermosetting resin whose refractive index was lower than that of E-glass fibres.

This study has demonstrated that it is possible to use the self-sensing concept to assess the full life-cycle of glass fibre composites.

In the first instance, the fracture behaviour of three classes of glass fibre bundles were investigated:

(a) as-received SDOF;

(b) heat-treated SDOF; and

(c) E-glass fibres.

(i) Custom designed end-tabs were used to enable fibre bundle to be loaded in tension without crushing them in the jaw of the tensile machine.

(ii) A technique was developed to monitor light intensity during tensile loading.

(iii) An acoustic machine transducer was surface mounted to monitor acoustic activity during tensile loading. The signal from the AE transducer was used to trigger the high-speed camera. It was demonstrated that the fracture of the fibre filament can be monitored within time during tensile loading with an accuracy of 95 ± 2 %.

Previous researchers have demonstrated that conventional E-glass fibre can be used as light guide to enable *in-situ* process monitoring and damage detection. The main achievements of this current study were as follows:

1. A technique was developed to enable the fabrication of void-free composite. This involved using mould manufactured from glass plate where the resin was injected using a motor-driven syringe and needle arrangement.
2. An intensity based technique was used to monitor the impregnation process which was shown in Section 3.4. As the resin filled the mould, the transmitted light intensity decreased significantly by ~80 %.
3. The same sample was processed in the oven and spectra were obtained to monitor the cross-linking process. It was shown that this technique was capable of monitoring cross-linking reaction.
4. Two types of fibre were used in the study namely: E-glass and SDOF. The SDOF were used to develop the production of void-free composite and the procedure to enable real-time damage detection during tensile loading.
5. An intensity-based technique was used to demonstrate that the temperature can be monitored during processing by tracking the transmitted light intensity through the SDOF. As the temperature was increased by 20 ^{0}C, the percentage increase in light transmission was ~20 %.
6. This study has demonstrated that SDOF can be used for monitoring the temperature and cross-linking process. Due to time constraint, the deployment for the use of damage detection was not undertaken.

Chapter 6

6.0 Recommendations for Future Research

In the current study, the fibre bundles were not coherent. The use of coherent fibre bundle will enable the fracture sequence of the individual filament to be monitored. This will give a new insight into fracture processes in composite.

With further research, it will be possible to relate the effect of surface treatment processing condition to the fracture mechanism in glass fibre composite.

The following future research is recommended:

1. The technique that was developed for void-free composites can be used to manufacture composites with a higher fibre volume fraction.
2. Thicker composite can be manufacture to enable other established tensile test method to be used including flexural, inter-laminar, and compressive loading.
3. The ability of SDOF to be used as intensity-based temperature sensors have to be extended to a higher temperature (up to 400 ^{0}C). The same should be evaluated for E-glass fibre.
4. Further work needed to be undertaken to improve laboratory impregnation process in particular, a technique have to be developed to enable constant volume filling of the mould. This is required to avoid the intermittent spikes that were observed when mould filling was being carried out.

References

1. Malik, S.A., Wang, L., Mahendran, R. S., Harris, D., Ojo, S. O., Collins, D., Paget, M., Pandita, S. D., Machavaram, V. R., & Fernando, G. F. *In-situ damage detection using self-sensing composites*. in *Sensors and smart structures technologies for civil, mechanical, and aerospace systems, San Diego CA , ETATS-UNIS (2009)*. 2009. San Diego, California, U.S.A: Society of Photo-Optical Instrumentation Engineers, Bellingham, WA, ETATS-UNIS.

2. Ruosi, A., *Nondestructive detection of damage in carbon fibre composites by SQUID magnetometry.* Physica Status Solidi, 2005. **2**(5): p. 1533-1555.

3. ISO 527-5:2009, *Plastics - Determination of tensile properties - Part 5: Test conditions for unidirectional fibre-reinforced plastic composites.* International Organisation for Standardisation, 2009(83.120: Reinforced Plastics): p. ISO 527-5.

4. Qiao, P., & Yang, M., *Fatigue life prediction pultruded E-glass/polyeurethane composites.* Journal of Composite Materials, 2004. **40**(9): p. 815-837.

5. Vladimirov, V.D., *Why not enlarge the non-destructive testing (NDT) experience in construction maintenance - Problems, Practice, Ideas, etc.?*, in *17th World Conference on Non-Destructive Testing*. 2008: Shanghai, China.

6. Grosse, C.U., & Krüger, M., *Inspection and monitoring of structures in civil engineering.* The E-Journal of Non-Destructive Testing, 2006. **11**(1).

7. Wang, S., Chung, D. D. L., & Chung, J. H., *Self-sensing of damage in carbon fiber polymer-matrix composite cylinder by electric resistance measurement.* Journal of Intelligent Material Systems and Structures, 2006. **17**: p. 00057-62.

8. Hayes, S., Liu, T., Brooks, D., Monteith, S., Ralph, B., Vickers, S. & Fernando, G. F., *In-situ self-sensing fiber reinforced composites.* Journal of Smart Materials and Structures, 1997. **6**: p. 432-440.

9. Fernando, G.F., *Fibre optic sensor systems for monitoring composite structures.* Journal of Reinforced Plastics, 2005. **49**(11): p. p. 41 - 49.

10. Tarnopol'skii, Y.M., & Kulakov, V. L., *Test methods for composites. Survey of investigation carried out in the PMI of Latvian academy of sciences in 1964 - 2000.* Journal of Mechanics of Composite Materials, 2001. **37**(5-6): p. 431-448.

11. Kister, G., Ralph, B., & Fernando, G. F., *Self-sensing E-glass fibres.* Journal of Optical Materials, 2002. **21** p. 713-727.

12. Bunsell, A.R., & Renard, J., *Series in material science and engineering - Fundamentals of fibre reinforced composite materials*. 2005, Bristol and Philadelphia: Institute of Physics Publishing.

13. Hull, D., & Clyne, W., *An introduction to composite materials*. Second ed. 1996, Cambridge: Cambridge university press.

14. BRE and Trend 2000 Ltd, *Polymer composites as construction materials*. 2001, BRE and Trend 2000 Ltd.

15. Halliwell, S.M., *Polymer composites in construction.* Journal of BRE Centre for Building Fabric, 2000. **405**.

16. Carter, C.B., & Norton, M. G., *Ceramic materials: Science and engineering*. 2007, New York: Springer Science Business Media.

17. Arhun, N., & Arman, A., *Fiber-reinforced technology in multidisciplinary chairside approaches.* Indian Journal of Dental Research, 2008. **19**(3): p. 272-277.

18. Catherall, J.A., *Fibre reinforcement*. First ed. 1973, London: Mills & Boon Limited.

19. Kruschandl, N., *Electrik publications and NJK*. 2006.

20. Structural Polymer Systems Ltd, *Composite materials handbook*. 1998, SP Systems.

21. Brown, E.N., Davis, A.K., Jonnalagadda, K.D., & Sottos, N.R., *Effect of surface treatment on the hydrolytic stability of E-glass fibre bundle tensile strength.* . Journal of Mechanics and Physics of Solids, 2004. **52**: p. 999-1022.

22. Searl, A., *A review of the durability of inhaled fibres and options for the design of series fibres.* The Annals of Occupational Hygiene, 1994. **38**(6): p. 839-855.

23. Perrot, Y., Baley, C., Grohens, Y., & Davies, P., *Damage resistance of composites based on glass fibre reinforced low styrene emission resins for marine applications.* Journal of Applied Composite Materials 2007. **14**(1): p. 67-87.

24. Liu, T., & Fernando, G. F., *Processing of polymer composites: an optical fibre-based sensor system for on-line amine monitoring composites Part A.* Journal of Applied Composite Materials, 2001. **32**(11): p. 1561-1572.

25. Thomas, W.F., *An investigation of the factors affecting the strength of glass fibre strand. Part 4. The effect of fibre surface area.* Journal of Glass Technology., 1972c. **13**(5): p. 141-144.

26. Thomas, W.F., *An investigation of the factors affecting the strength of glass fibre strand. Part 3. The strength in polyester resin.* Journal of Glass Technology., 1972b. **13**(4): p. 122-125.

27. Thomas, W.F., *An investigation of the factors affecting the strength of glass fibre strand. Part 2.* Journal of Glass Technology., 1972a. **13**(1): p. 17-21.

28. Thomas, W.F., *An investigation of the factors affecting the strength of glass fibre strand.* Journal of Glass Technology, 1971. **12**(3): p. 60-64.

29. Dibenedetto, A.T., & Lex, P. J., *Evaluation of surface treatments for glass fibers in composite materials.* Journal of Polymer Engineering and Science 2004. **29**(8): p. 543-555.

30. Okoroafor, E.U., & Hill, R., *Determination of fibre-resin interface strength in fibre-reinforced plastics using the acoustic emission technique* Journal of Applied Physics D: The Applied Physics, 1995. **28**(9): p. 1816.

31. Harris, B., *A perspective view of composite materials development* Journal of Materials and Design 1991. **12** (5): p. 259-272.

32. Motavalli, M., *Materials properties - Fibre composites FS10*, in *Materials and properties of polymer matrix composites*. 2008.

33. Callister. Jr, W.D., *Material science and engineering an introduction*. Seventh ed. 2007, U.S.A.: John Wiley & Sons, Inc.

34. Crosby, P.A., & Fernando, G. F., *Cure monitoring, Optical fibre sensor technology.* , in *The application of optical fibre sensors in advanced fibre reinforced composites.*, K.T.V.M. Grattan, B. T. , Editor. 1999, Kluwer Academic Publishers.

35. Gooch, J.W., *Encyclopedic dictionary of polymers*. 2007, Springer Science Business Media, LLC.: Atlanta.

36. Fernando, G.F., & Degamber, B., *Process monitoring of fibre reinforced composites using optical fibre sensors.* Journal of Institute of Materials, Minerals and Minings and ASM International, 2006. **51**(2).

37. Fernando, G.F., *Fiber optic sensor systems for monitoring composite structures.* Reinforced Plastics, 2005. **49**(11): p. 41-49.

38. Fernando, G.F., and Degamber, B., *Process monitoring of fibre reinforced composites using optical fibre sensors.* Institute of Materials, Mineral and Minings and ASM International, 2006. **51**(2).

39. Thyagarajan, K., & Ghatak, A., *Fiber optics.essentials*. 2007, New Jersey: John Wiley and Son Inc.

40. Lau, K., Chan, C., Zhou, L., and Jin, W., *Strain monitoring in composite-strengthened concrete structures using optical fibre sensors.* Composites Part B: Engineering, 2001. **32**(1): p. 33-45.

41. Shin, M., *Fibre optic sensors* 2008, University of Illinois, Urbana-Champaign, U.S.A.

42. Muhs, J.D., *Fiber Optic Sensor: Providing cost effective solutions industry needs.* 2002, Oak Ridge National Laboratory.

43. Gholamzadeh, B., & Nabovati, H., *Fiber optic sensors*, in *Proceedings of World Academy of Science, Engineering and Technology*. 2008: Iran.

44. Lau, K.T., *Fibre-optic sensors and smart composites for concrete applications*, in *Magazine of Concrete Research*. 2003. p. 19-34.

45. Leng, J.S., Winter, D., Barnes, R. A., Mays, G. C., & Fernando, G. F., *Structural helth monitoring of smart civil structures using fibre optic sensors*, in *The 3rd International Conference on Experimental Mechanics*. 2005, SPIE - The International Society of Optical Engineers: Singapore.

46. Pan, X., Liang, D., and Dongsheng, L., *Optical fiber sensor layer embedded in smart composite material and structure* Journal of Smart Materials and Structures, 2006. **15**(5).

47. Kister, G., Ralph, J.D.R., & Fernando, G. F., *Damage detection in glass fibre-reinforced plastic composites using self-sensing E-glass fibres.* Journal of smart materials and structures, 2003. **13**: p. 1166 -1175.

48. Wang, L., Kister, G., Ralph, B., Talbot, J. D. R., & Fernando, G. F., *Conventional E-glass fiber light guides: Self-sensing composite based on Sol-gel cladding.* Journal of Smart Materials and Structures, 2003. **13**: p. 73-81.

49. Kister, G., Badcock, G., & Fernando, G. F., *A novel technique to study the fracture of E-glass fiber reinforced composites.* Journal of Material Science and Engineering, 2004. **39**: p. 1425-428.

50. Xu, L., Fu, J. H. & Schlup, J. R., *In Situ Near-Infrared Spectroscopic Investigation of the Kinetics and Mechanisms of Reactions between Phenyl Glycidyl Ether (PGE) and Multifunctional Aromatic Amines.* Industrial & Engineering Chemistry Research, 1996. **35**(3): p. 963–972.

51. Powell, K.D., Ghaemmaghami, S., Wang, M. Z., Ma, L., Oas, T. G., & Fitzgerald, M. C., *A general mass spectrometry based assay for the quantitation of protein-ligand binding interactions in solution.* Journal of American Chemical Society, 2002. **124**: p. 10256-10257.

52. Wong, S.F., Meng, C. K., & Fenn, J. B., *Multiple changing in electrospray ionization of poly(ethylene glycol).* Journal of Physical Chemistry, 1988. **92**: p. 546-550.

53. Bikiaris, D., Matzinos, P., Larena, A., Flaris, V., & Panayiotou, C., *Use of silane agents and poly(propylene - g - maleic anhydride) copolymer as adhesion promoters in glass fiber/polypropylene composites.* Journal of Applied Polymer Science, 2001. **81**(3): p. 701-709.

54. Lin, T., Wang, K., Wang, X., & Kaynak, A., *Polymerising pyrrole on polyester textiles and controlling the conductivity through coating thickness.* Journal of Thin Solid Films, 2005. **479**: p. 77-82.

55. R'Mili, M., Moevus, M. & Godin, N., *Statistical fracture of E-glass fibres using a bundle tensile test and acoustic emission monitoring.* Composites Science and Technology, 2008. **68**(2008): p. 1800-1808.

56. Mancini, S., Tumino, G., & Gaudenzi, P., *Structural health monitoring for future Space vehicles.* Journal of Intelligent Material Systems and Structures, 2006. **17**(577).

57. Sato, N., & Karauchi, T., *Interpretation of acoustic emission signal from composite materials and its application to design of automotive composite components.* Toyota Central Research and Development Laboratories Inc., Nagakute, Aichi-gun, Aichi, 480-11, Japan, 1997. **9**(Res Nondestr Eval): p. 119-36.

58. Tsutsui, H., Kawamata, A., Sanda, T., & Takeda, N., *Detection of impact damage of stiffened composite panels using embedded small-diameter optical fibers.* Smart Materials and structures, 2004. **13**(6): p. 1284.